BRNO UNIVERSITY OF TECHNOLOGY

Faculty of Electrical Engineering
and Communication

MASTER'S THESIS

Brno, 2019 Bc. Yaroslav Saprykin

BRNO UNIVERSITY OF TECHNOLOGY

VYSOKÉ UČENÍ TECHNICKÉ V BRNĚ

FACULTY OF ELECTRICAL ENGINEERING AND COMMUNICATION

FAKULTA ELEKTROTECHNIKY
A KOMUNIKAČNÍCH TECHNOLOGIÍ

DEPARTMENT OF RADIO ELECTRONICS

ÚSTAV RADIOELEKTRONIKY

MODEL OF PHYSICAL LAYER OF COMMUNICATION SYSTEM IEEE 802.11AF

MODEL FYZICKÉ VRSTVY KOMUNIKAČNÍHO SYSTÉMU IEEE 802.11AF

MASTER'S THESIS
DIPLOMOVÁ PRÁCE

AUTHOR — **Bc. Yaroslav Saprykin**
AUTOR PRÁCE

SUPERVISOR — **doc. Ing. Ladislav Polák, Ph.D.**
VEDOUCÍ PRÁCE

BRNO 2019

VYSOKÉ UČENÍ TECHNICKÉ V BRNĚ
FAKULTA ELEKTROTECHNIKY A KOMUNIKAČNÍCH TECHNOLOGIÍ

Diplomová práce

magisterský navazující studijní obor **Elektronika a sdělovací technika**
Ústav radioelektroniky

Student: Bc. Yaroslav Saprykin ***ID:*** 158222
Ročník: 2 ***Akademický rok:*** 2018/19

NÁZEV TÉMATU:

Model fyzické vrstvy komunikačního systému IEEE 802.11af

POKYNY PRO VYPRACOVÁNÍ:

V teoretické části práce prostudujte vlastnosti bezdrátového komunikačního systému IEEE 802.11af. Zaměřte se na způsob zpracování signálu na fyzické vrstvě a seznamte s možnostmi jejich matematického popisu. Uvažujte různé systémové nastavení, případně vysílací módy, a různé modely přenosových kanálů. V programu MATLAB vytvořte základní simulační model (vysílač a přijímač) s nastavitelnými parametry fyzické vrstvy IEEE 802.11af.

V realizační části práce navrhněte aplikaci s grafickým rozhraním v prostředí MATLAB, umožňující simulaci vlivu přenosového kanálu na IEEE 802.11af signál. Zaměřte se na různé modely přenosových kanálů. Správnost vytvořeného modelu ověřte simulací a zhodnoťte vliv systémových parametrů IEEE 802.11af na dosaženou chybovost a kvalitu přenosu. Získané výsledky vyhodnoťte a proveďte jejich rozbor.

DOPORUČENÁ LITERATURA:

[1] LEKOMTCEV, D., MARSALEK, R. Comparison of 802.11af and 802.22 standards – physical layer and cognitive functionality. Elektrorevue, 2012, vol. 3, no. 2, pp. 12-18.

[2] MILOS, J. et. al. Link-Level Simulator for WLAN Networks. On the 1st International Workshop on Link-and System Level Simulations (IWSLS²). Vienna (Austria), 2016. pp. 1-4.

Termín zadání: 4.2.2019 ***Termín odevzdání:*** 16.5.2019

Vedoucí práce: doc. Ing. Ladislav Polák, Ph.D.
Konzultant:

prof. Ing. Tomáš Kratochvíl, Ph.D.
předseda oborové rady

ABSTRACT

This diploma thesis deals with modeling, simulation and analysis of the IEEE 802.11af wireless communication system on the physical layer. The work primarily describes the transmitting part of the communication system with an emphasis on the processing IEEE 802.11af signal. Subsequently, the block diagram and the basic model are created for the transmitting and receiving parts in SISO and MIMO transmission modes. The PHY model of IEEE 802.11af, with a graphical user interface (GUI), is created in MATLAB program environment. This application is used to explore the features and performance of the IEEE 802.11af based on its system parameters. System parameters can be configured by a user and different transmission scenarios can be simulated.

KEYWORDS

IEEE 802.11af, TVWS, fading channels, signal processing, OFDM, PHY layer

ABSTRAKT

Tato diplomová práce se zabývá analýzou, návrhem a simulací modelu fyzické vrstvy bezdrátového komunikačního systému IEEE 802.11af. V práci je především popsána vysílací část komunikačního systému s důrazem na zpracování IEEE 802.11af signálu. Následně je vytvořeno blokové schéma a model pro vysílací a přijímací části ve vysílacích módech SISO a MIMO. Model je realizován s grafickým uživatelským rozhraním v programovém prostředí MATLAB. Vytvořená aplikace slouží k prozkoumání vlastností IEEE 802.11af modelu na základě jeho systémových parametrů. Systémové parametry jsou volitelné uživatelem a aplikace poskytuje možnost simulace různých přenosových scénářů.

KLÍČOVÁ SLOVA

IEEE 802.11af, TVWS, fading channels, signálové zpracování, OFDM, PHY vrstva

SAPRYKIN, Yaroslav. *Model of physical layer of communication system IEEE 802.11af*. Brno, 2019, 87 p. Master's Thesis. Brno University of Technology, Faculty of Electrical Engineering and Communication, Department of Radio Electronics. Advised by doc. Ing. Ladislav Polák, Ph.D.

DECLARATION

I declare that I have written the Master's Thesis titled "Model of physical layer of communication system IEEE 802.11af" independently, under the guidance of the advisor and using exclusively the technical references and other sources of information cited in the thesis and listed in the comprehensive bibliography at the end of the thesis.

As the author I furthermore declare that, with respect to the creation of this Master's Thesis, I have not infringed any copyright or violated anyone's personal and/or ownership rights. In this context, I am fully aware of the consequences of breaking Regulation § 11 of the Copyright Act No. 121/2000 Coll. of the Czech Republic, as amended, and of any breach of rights related to intellectual property or introduced within amendments to relevant Acts such as the Intellectual Property Act or the Criminal Code, Act No. 40/2009 Coll., Section 2, Head VI, Part 4.

Brno ....

author's signature

ACKNOWLEDGEMENT

I would like to thank my supervisor doc. Ing. Ladislav Polák, Ph.D. He has supported and inspired me throughout my master thesis with their patience and knowledge. This work would have never been completed without his support.

Brno ....

author's signature

Faculty of Electrical Engineering
and Communication
Brno University of Technology
Purkynova 118, CZ-61200 Brno
Czech Republic
http://www.six.feec.vutbr.cz

ACKNOWLEDGEMENT

Research described in this Master's Thesis has been implemented in the laboratories supported by the SIX project; reg. no. CZ.1.05/2.1.00/03.0072, operational program Výzkum a vývoj pro inovace.

Brno ....
author's signature

EVROPSKÁ UNIE
EVROPSKÝ FOND PRO REGIONÁLNÍ ROZVOJ
INVESTICE DO VAŠÍ BUDOUCNOSTI

Contents

Introduction **14**

1 Standard IEEE 802.11af **15**
1.1 Architecture basics . . . 16
1.2 Basic Mechanisms . . . 18

2 Physical layer of IEEE 802.11af **20**
2.1 802.11af PHY scheme . . . 21
2.2 PPDU format . . . 24
2.3 Scrambler . . . 26
2.4 Convolutional encoder . . . 26
2.5 LDPC encoder . . . 28
2.6 Interleaving . . . 28
2.7 OFDM modulation . . . 29
2.7.1 Subcarrier modulation . . . 30
2.7.2 Pilot subcarriers . . . 31
2.7.3 Creating OFDM symbols . . . 32
2.8 MIMO . . . 34
2.8.1 Space-Time Block Codes (STBC) . . . 36
2.8.2 Cyclic Shift Diversity (CSD) . . . 37
2.9 Channel transmission models . . . 38
2.9.1 Additive White Gaussian Noise (AWGN) channel . . . 38
2.9.2 Rician channel . . . 38
2.9.3 Rayleigh channel . . . 40
2.9.4 Pedestrian Indoor channel . . . 40
2.10 Equalization . . . 40
2.10.1 Zero Forcing . . . 41

3 Program description **42**
3.1 Block diagram model . . . 42
3.2 Transmitter . . . 43
3.2.1 Creating of IEEE 802.11af frame structure . . . 43
3.2.2 Data scrambling . . . 43
3.2.3 Data encoding . . . 44
3.2.4 Data interleaving . . . 44
3.2.5 Subcarrier mapping . . . 44
3.2.6 STBC encoder . . . 45

3.2.7 OFDM mapping . . . 45
3.2.8 RRC filtering . . . 46
3.2.9 IQ modulation . . . 46
3.3 Transmission channel . . . 46
3.4 Receiver . . . 48
3.4.1 IQ demodulation . . . 48
3.4.2 RRC defiltering . . . 48
3.4.3 OFDM demapping . . . 48
3.4.4 STBC decoder . . . 49
3.4.5 Subcarrier demapping . . . 49
3.4.6 Data deinterleaving . . . 50
3.4.7 Data decoding . . . 50
3.4.8 Data descrambling . . . 50
3.5 GUI description . . . 51

4 Simulation results **53**
4.1 Test conditions . . . 53
4.2 Simulation in AWGN channel . . . 54
4.2.1 BER . . . 54
4.2.2 MER . . . 57
4.2.3 Frequency spectrum . . . 58
4.2.4 Constellation diagram . . . 59
4.3 Simulation in Rician channel . . . 59
4.3.1 BER . . . 60
4.3.2 MER . . . 62
4.3.3 Frequency spectrum . . . 64
4.3.4 Constellation diagram . . . 64
4.4 Simulation in Rayleigh channel . . . 66
4.4.1 BER . . . 66
4.4.2 MER . . . 69
4.4.3 Frequency spectrum . . . 70
4.4.4 Constellation diagram . . . 71
4.5 Simulation in MIMO 2x2 mode . . . 72
4.5.1 BER . . . 72

5 Conclusion **75**

Bibliography **77**

List of symbols, physical constants and abbreviations **80**

List of appendices **84**

A Parameters for VHT mode **85**

A.1 Timing-related constants 85
A.2 Modulation-dependent parameters 85
A.3 Number of rows and columns in the interleaver 85
A.4 First permutation rule 85
A.5 Second permutation rule 86
A.6 Pilots mapping for BCU 6 and 8 MHz 86
A.7 Pilots mapping for BCU 7 MHz 86
A.8 Data subcarriers mapping for BCU 6 and 8 MHz 86
A.9 Data subcarriers mapping for BCU 7 MHz 87

List of Figures

1.1 System architecture including all components of the IEEE 802.11af standard. . . . 16
2.1 The TVHT channel configuration for the W, 2W, W+W a 2W+2W modes. . . . 20
2.2 Transmitter block diagram. . . . 22
2.3 PPDU format. . . . 25
2.4 SIGNAL field bit assignment. . . . 25
2.5 Data scrambler. . . . 26
2.6 Convolutional encoder. . . . 27
2.7 Example of the bit-stealing and bit-insertion procedure for the coding rate $R = 3/4$. . . . 27
2.8 OFDM symbols orthogonality. . . . 29
2.9 OFDM modulator. . . . 30
2.10 BPSK, QPSK, and 16-QAM constellation bit encoding. . . . 31
2.11 Subcarrier frequency allocation. . . . 34
2.12 MIMO system scheme. . . . 35
2.13 MIMO 2x2 system scheme. . . . 36
2.14 AWGN channel. . . . 38
2.15 Zero Forcing equalization. . . . 41
3.1 Block diagram of the IEEE 802.11af communication model in MATLAB. 42
3.2 Simulation of the IEEE 802.11af transmitter model. . . . 51
4.1 BER before Viterbi decoding for the BPSK, QPSK, 16QAM and 64QAM modulations in the duplicate non-HT mode in the AWGN channel. . . . 55
4.2 BER before Viterbi decoding for the BPSK, QPSK, 16QAM, 64QAM and 256QAM modulations in the VHT mode in the AWGN channel. . 55
4.3 BER after Viterbi decoding for the BPSK, QPSK, 16QAM and 64QAM modulations in the duplicate non-HT mode in the AWGN channel. . 56
4.4 BER after Viterbi decoding for the BPSK, QPSK, 16QAM, 64QAM and 256QAM modulations in the VHT mode in the AWGN channel. . 57
4.5 MER for the BPSK, QPSK, 16QAM and 64QAM modulations in the duplicate non-HT mode in the AWGN channel. . . . 58
4.6 MER for the BPSK, QPSK, 16QAM, 64QAM and 256QAM modulations in the VHT mode in the AWGN channel. . . . 58
4.7 Baseband frequency spectrum in the duplicate non-HT mode in the AWGN channel . . . 59

4.8 Constellation diagrams in the duplicate non-HT mode in the AWGN channel . . . 59
4.9 BER before Viterbi decoding for the BPSK, QPSK, 16QAM and 64QAM modulations in the duplicate non-HT mode in the Rician channel. . . . 60
4.10 BER before Viterbi decoding for the BPSK, QPSK, 16QAM, 64QAM and 256QAM modulations in the VHT mode in the Rician channel. . . 61
4.11 BER after Viterbi decoding for the BPSK, QPSK, 16QAM and 64QAM modulations in the duplicate non-HT mode in the Rician channel. . . 62
4.12 BER after Viterbi decoding for the BPSK, QPSK, 16QAM, 64QAM and 256QAM modulations in the VHT mode in the Rician channel. . 62
4.13 MER for the BPSK, QPSK, 16QAM and 64QAM modulations in the duplicate non-HT mode in the Rician channel. . . . 63
4.14 MER for the BPSK, QPSK, 16QAM, 64QAM and 256QAM modulations in the VHT mode in the Rician channel. . . . 64
4.15 Baseband frequency spectrum in the duplicate non-HT mode in the Rician channel . . . 64
4.16 Constellation diagrams in the duplicate non-HT mode in the Rician channel without ZF equalization . . . 65
4.17 Constellation diagrams in the duplicate non-HT mode in the Rician channel with ZF equalization . . . 66
4.18 BER before Viterbi decoding for the BPSK, QPSK, 16QAM and 64QAM modulations in the duplicate non-HT mode in the Rayleigh channel. . . . 67
4.19 BER before Viterbi decoding for the BPSK, QPSK, 16QAM, 64QAM and 256QAM modulations in the VHT mode in the Rayleigh channel. 67
4.20 BER after Viterbi decoding for the BPSK, QPSK, 16QAM and 64QAM modulations in the duplicate non-HT mode in the Rayleigh channel. . 68
4.21 BER after Viterbi decoding for the BPSK, QPSK, 16QAM, 64QAM and 256QAM modulations in the VHT mode in the Rayleigh channel. 69
4.22 MER for the BPSK, QPSK, 16QAM and 64QAM modulations in the duplicate non-HT mode in the Rayleigh channel. . . . 70
4.23 MER for the BPSK, QPSK, 16QAM, 64QAM and 256QAM modulations in the VHT mode in the Rayleigh channel. . . . 70
4.24 Baseband frequency spectrum in the duplicate non-HT mode in the Rayleigh channel . . . 71
4.25 Constellation diagrams in the duplicate non-HT mode in the Rayleigh channel without ZF equalization . . . 72

4.26 Constellation diagrams in the duplicate non-HT mode in the Rayleigh channel with ZF equalization 72
4.27 Comparison of BER before Viterbi decoding between MIMO 2x2 and SISO antenna modes for the MCS indexes 0 and 3 in the duplicate non-HT mode in the AWGN channel. 73
4.28 Comparison of BER after Viterbi decoding between MIMO 2x2 and SISO antenna modes for the MCS indexes 0 and 3 in the duplicate non-HT mode in the AWGN channel. 74

List of Tables

2.1 Modulation-dependent parameters for Non-HT duplicate mode. . . . 23
2.2 Timing-related constants in Non-HT PPDU. 24
2.3 Modulation-dependent normalization factor K_{MOD}. 30
2.4 Pilots mapping for BCU 6 and 8 MHz. 32
2.5 Pilots mapping for BCU 7 MHz. 32
2.6 Data mapping for BCU 6 and 8 MHz. 33
2.7 Data mapping for BCU 7 MHz. 33
2.8 Fading parameters for RC12 and RA12 channel models. 39
2.9 Fading parameters for PI12 channel model. 40

Introduction

Nowadays, interest in commercial known Wi-Fi (Wireless-Fidelity) technology is rapidly increasing. The basics of this technology were already described in the IEEE (Institute of Electrical and Electronics Engineers) 802.11 standard in 1997. In general, the IEEE 802.11 standard is a group of IEEE standards for WLAN (Wireless Local Area Network) implementation. Each of these standards is a set of PHY (Physical Layer) and MAC (Medium Access Control Sublayer) specifications which describes a WLAN network. Traditionally, the IEEE 802.11 standard provides wireless connectivity mostly for short-range applications where the communicating devices are plugged in. However, these are not ideal circumstances for many IoT (Internet of Things) applications that demand both longer signal distances and lower power consumption in mobile devices [1].

The IEEE 802.11af standard is one of the newer standards in the family of IEEE 802.11 which is approved in 2014. Unlike IEEE 802.11a/b/g/n/ac standards which are utilized in the ISM (Industrial, Scientific and Medical) band in GHz units, the IEEE 802.11af standard allows WLAN services in additional radio band and the gaps of not used TV (Television) spectrum. Such field of the spectrum is called TVWS (TV White Spaces). In Europe, according to ETSI (European Telecommunications Standards Institute), the TVWS spectrum is defined in UHF (Ultra High Frequency) band on a frequency range 490-790 MHz. In the USA according to FCC (Federal Communications Commission) TVWS spectrum is defined in VHF (Very High Frequency) and UHF bands on frequency range 54-698 MHz [1],[2],[3].

The main purpose of this diploma thesis is to design the simulation model based on the IEEE 802.11af standard in the MATLAB program environment. Further, the simulation results of such a designed model will be simulated in dependence on its system parameters and analyzed. This model consisting of a transmitter, fading channel model and receiver will give the opportunity to test influence on the IEEE 802.11af system robustness affected by system parameters choice. The diploma thesis emphasis is on PHY of the IEEE 802.11af standard.

In the first chapter mentioned basic motivation for the IEEE 802.11af standard birth, designing of the concept and its advantages. Besides, it is describing the basic components of the standard and its architecture. Then are described basic application mechanisms. In the second chapter are described basic components of the system at PHY. Further, it describes fading models of the transmission channel. The third chapter describes a whole model implementation which is consist of components described in the second chapter. Besides, it describes the created program and shows the functionality of the simulation model. In the last chapter are described and analyzed the results of simulations in the created application.

1 Standard IEEE 802.11af

To avoid interference between high-powered stations have to be a sufficient area between its coverage. Such areas could be used for low-powered Wi-Fi access points which do not radiate so far and could securely work without interference. Research for using radio spectrum in such a way is going on for a long time. Regulation authorities try to implement this solution mainly because of the spectrum using efficiency [4].

The concept of the IEEE 802.11af standard relies on access point ability to transmit a low-power Wi-Fi signal in the area which is located between the primary broadcast transmitters working on the same radio channel [4].

The broadcast system is designed to have a sufficient reserve gap between TV broadcast transmitters coverage. Such a gap could guaranty interference-free reception also in case of tropospheric conditions for transmission on far distances. In areas between such transmitters, could be used low-powered small transmitters [4].

Since the use of channels varies, the access point has to know which channel it can use. To gain this goal can be used different technics. No matter what technic is used, an IEEE 802.11af access point has to be automatically reconfigurable [4].

For access points, which are requested low power consumption, can be applied not used radio spectrum between TV transmitters coverage areas [4].

There are many advantages for the IEEE 802.11af system starting from using TVWS spectrum. Whereas the IEEE 802.11af system uses frequency 1 GHz below what allows signals to gain long distance at the transmission. Current Wi-Fi systems use frequency in the range of Industrial, Scientific and Medical (ISM) band where are signals easily absorbed by obstacles [4].

One of the advantages is access to unused TV spectrum. To work with IEEE 802.11af technology has to be ensured that the system will avoid unreasonable interference with coexisting TV transmissions. Existing technologies and rules could be used to achieve this. One of these technologies is cognitive radio [5]. That allows the IEEE 802.11af system to detect transmissions and to switch to available channels [5]. The next technology is geographic scanning. With the geographic database and knowledge of channel availability system will give the opportunity to avoid using of occupied channels [4].

1.1 Architecture basics

In this part are described system architecture used for the IEEE 802.11af standard and its key components [1].

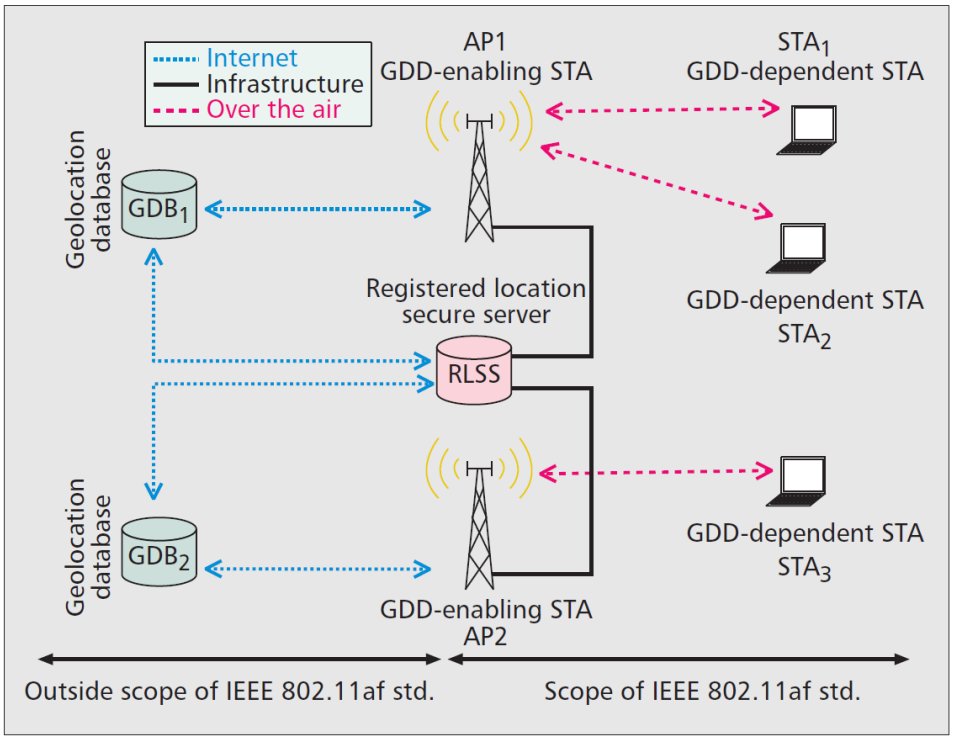

Fig. 1.1: System architecture including all components of the IEEE 802.11af standard [1].

According to Fig. 1.1 GDB (Geolocation Database) is the primary component in the IEEE 802.11af system. This component makes the main difference from other IEEE 802.11 standards. The GDB is a database which contains permitted frequencies and operating parameters for a WSDs (White Space Device) to fulfill regulatory requirements in dependence on geographical location. The GDB is authorized and controlled by regulatory authorities. A GDB's operation depends on the safety and time requirements in the actual regulatory domain [1],[6].

RLSS (Registered Location Secure Server) is the next component of the network architecture used in the IEEE 802.11af standard. Such entity operates like a local database consisting of a geographic location and operating parameters for the small number of basic services called BSSs (Basic Service Set). RLSS distributes allowed operation parameters to the APs (Access Point) and STAs (Station) within BSSs under the RLSS's control. The role of the RLSS can vary on the used approach in the system [1].

GDD (Geolocation-Database-Dependent) entities are remaining components in the IEEE 802.11af architecture. GDD operations are controlled by an authorized GDB to fulfill regulatory requirements. In the IEEE 802.11af architecture under the GDD have defined two types of entities [1].

The first one is called GDD-enabling STA which is the equivalent entity to a known AP. The second one is called GDD-dependent STA which basically means STA. In the IEEE 802.11af standard, the GDD-enabling STA entity controls the GDD-dependent STAs operation in its BSS service. A GDD-enabling STA allows secure access to the GDB to obtain transmitting frequency and permitted parameters in the coverage area. Such information allows a GDD-enabling STA to be an authority for enabling and control a GDD-dependent STA operation under its service. The parameters which a GDD-enabling STA obtains from the GDB are represented through a WSM (White Space Map). The maintenance and distribution of a valid WSM are ensured by the GDD-enabling STA. Besides a GDD-enabling STA transmits a CVS (Contact Verification Signal) for GDD-dependent STAs to check the validity of the WSM. Each GDD-dependent STA could obtain the permitted operating frequencies and parameters in the form of a WSM in two ways: from GDD-enabling STAs or directly from the RLSS. The validity of the WSM is confirmed through the CVS transmitted by the GDD-enabling STA. The communication between GDD-enabling STA and GDD-dependent STA is implemented via RLQP (Registered Location Query Protocol) which allows operation of the main mechanisms used in the IEEE 802.11af standard. This protocol allows sharing a WSM and channel utilization for the STAs [1].

It is important to note that a GDB provides information in the form of WSM to WSDs. Each WSM contains identified available TWVS channels and corresponding power limitations. Before GDD-enabling STA transmission begins, it requires to obtain the WSM from GDB. Further, the GDD-enabling STA generates the WSM which is transmitted to the GDD-dependent STAs related to the operating region. The WSM is transmitted by the GDD-enabling STA throughout frames which are related to the IEEE 802.11af mechanisms. Moreover, when the channel bandwidth consists of multiple TVWS channels, transmission power limitation in a WSM selected as the minimum power level of the channels. Concerning the transmitting channel, the GDD-dependent STAs can only transmit on the available channels according to the valid WSM. Furthermore, the WSM can be updated by the GDB due to channel availability changes. In such case, GDD-dependent STA obtains an updated WSM from GDD-enabling STA and adjusts its operating channel due to the updated WSM. Besides, the 802.11af standard describes the general format of the WSM which can be applied to any regulatory domain [1].

According to Fig. 1.1 the communication between the GDB and RLSS entities is

independent on the IEEE 802.11af standard protocol and solved by the regulator's protocol over the Internet's infrastructure. As shown in Fig 1.1 the communication between the GDD-enabling STAs and the RLSS is bidirectional through over infrastructure. The communication between the GDD-enabling STAs and GDD-dependent STAs is bidirectional over-the-air communication in TVWS or other ISM bands [1].

1.2 Basic Mechanisms

In this part are described mechanisms defined in the IEEE 802.11af standard [1].

CAQ (Channel Availability Query) is the mechanism which allows the STAs to obtain the available radio frequencies to operate in their coverage area in the format of WSM. During the CAQ procedure, the RLSS grants the WSM to the requesting STA. In some regulatory domains, the RLSS requests the GDB first to obtain a WSM. There are three different cases when the GDD-dependent STA process a CAQ request to the GDD-enabling STA. First, to stay in the GDD enable state after enablement times out. Second, when a change in channel availability triggered using CVS by the GDD-enabling STA. Third, when a GDD-dependent STA has moved from the regulatory permitted distance [1].

The next mechanism is the CSM (Channel Schedule Management) which allows the GDD-enabling STAs to query other GDD-enabling STAs or the RLSS to obtain white space channel schedule information. Such information contains the start and end times for the requested channels. Important to note that GDD-enabling STAs can transmit a CSM request to other GDD-enabling STAs or the RLSS except GDD-dependent STAs [1].

For the recognition which the GDD-dependent STAs are in the reception zone from the GDD-enabling STA used CVS (Contact Verification Signal). In addition, this signal helps to ensure that the GDD-dependent STAs are operating under a valid WSM. The GDD-dependent STAs receives a CVS frames with map ID field. In the case of received map ID value is equals to map ID value from existing WSM, the GDD-dependent STA counts operating WSM as a valid and enablement validation timer resets. In the case, if received map ID value is different from the existing map ID value, the GDD-dependent STA transmits a CAQ request for obtaining the valid WSM. If the GDD-dependent STA does not receive the valid WSM, it stops transmission after the enablement validation timer is expired [1].

To form a network according to regulatory requirements under the control of the GDB throughout the GDD-enabling STA has used the GDD Enablement mechanism. The GDB-enabling STA transmits a GDD beacon signal on available channels in the TVWS band to offer the GDD enablement service. When the GDD-dependent

STA receives the GDD beacon signal, it can attempt enablement with the GDD Enablement Response frame. For the GDD-dependent STAs are defined three GDD enablement states: GDD Enabled, Attempting GDD Enablement, and unenabled. After the GDD-dependent STA is received a successful GDD Enablement Response, the GDD Enabled state is activated. When the GDD-dependent STA receives a GDD-enabling signal that allows it only to transmit the GDD enabling response frame after GDB authentication, it will activate Attempting GDD Enablement state. If the GDD-dependent STA cannot transmit any frames except passively scanning of channels for an enabling signal from the GDD-enabling STA, then it has the unenabled state [1].

In addition, two main causes could be found when the GDD-dependent STA state changes from GDD Enabled to unenabled. First, WSM, CVS and CAQ procedures perform GDD enablement validity timer modification. Therefore, GDD timer is expired and GDD-dependent STA is switched to the unenabled state. Second, a GDD-dependent STA transmission is interrupted by the GDD-enablement STA [1].

To control the frequency utilization in the TVWS band is used a two-message procedure called the NCC (Network Channel Control). This procedure is commonly used between STAs in the next way. The GDD-dependent STA plays the role of NCC requesting STA, and the GDD-enabling STA plays the role of NCC responding STA. Basically, the spectrum mask related to the WSM is provided by NCC requesting STA to check the utilization of selected frequencies. When an NCC response frame contains the valid network channels and related transmit power constraints, the NCC responding STA will allow operation in the requested frequencies. In addition, a new NCC request can be performed whenever the WSM is changed [1].

As a result, the IEEE 802.11af system provides advantages of using frequency channels in the TVWS band. Furthermore, the using of frequency under 1 GHz allows better penetration throughout obstacles and better coverage area than it is possible in the ISM band. However, the IEEE 802.11af system requires sophisticated architecture containing GDB, RLSS, and GDD entities. The communication between its entities is implemented via five basic mechanisms CAQ, CSM, CVS, GDD enablement, and NCC. The information regarding the TVWS band transmitted in a WSM [1].

2 Physical layer of IEEE 802.11af

The physical layer for the TVHT (Television Very High Throughput) system is defined by the IEEE 802.11af standard [7]. The TVHT system is derived from the OFDM (Orthogonal Frequency Division Multiplexing) system. Basic components of the IEEE 802.11af communication system will be described and based on the OFDM system. In comparison with previous IEEE 802.11 standards, the IEEE 802.11af standard uses the WSDs operating in the TVWS band. According to the regulatory authority is allowed using the Basic Channel Unit (BCU) with bandwidth 6, 7 or 8MHz for the TVHT equipment. In addition, bonded (2W or 4W) and non-contiguous (W+W or 2W+2W) bandwidths are supported according to Fig. 2.1 where the W (Width) means the single-channel bandwidth. The TVHT channel configuration is defined by the W, 2W, W+W, 2W+2W modes [7].

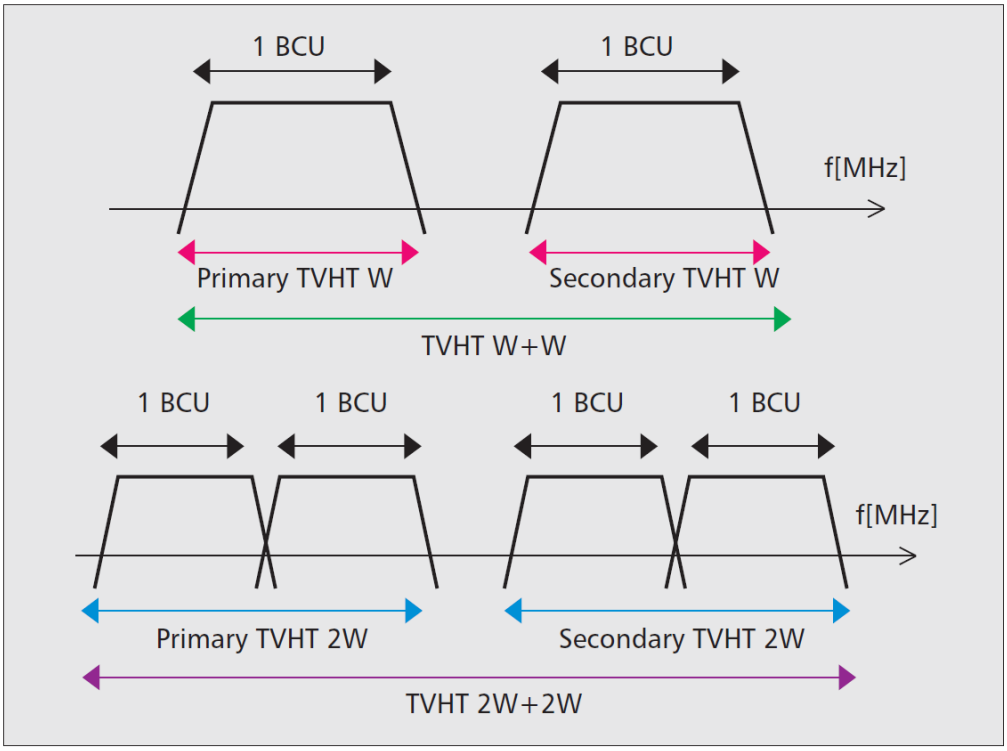

Fig. 2.1: The TVHT channel configuration for the W, 2W, W+W a 2W+2W modes [7].

Only the single-channel bandwidth and the single spatial stream are mandatory. Basically, the MIMO (Multiple-Input-Multiple-Output) transmission for the 4x4 system configuration using four STBC (Space-Time Block Coding) blocks are supported. Moreover, 4x MU (Multi-User) diversity are supported [7].

The TVHT format of the transmission is similar to 40 MHz VHT (Very High Throughput) transmission. It defines 144 OFDM subcarriers for 6 and 8 MHz channels and 168 OFDM subcarriers for 7 MHz channel. Transmissions for 6 and 7 MHz channels are spectrally identical. For each W data are transmitted on subcarrier indexes from -58 to -2 and from 2 to 58. On the subcarrier indexes +-11, +-25 and +-53 are allocated 6 pilots. The subcarrier index 0 forms the DC (Direct Current) part of the TVHT signal. In the case of more frequency segments (2W, W+W, 2W+2W) the subcarriers as described upper are duplicated [7].

The TVHT STA has to support the next functions [7]:

- TVHT_MODE_1 (1x BCU)
- Simple spatial stream MCSs (Modulation and Coding Scheme) from 0 to 7 (for transmission and reception)
- Binary convolutional coding
- The normal and short guard interval (for transmission and reception)

The TVHT STA may support the next functions [7]:

- TVHT_MODE_2C, TVHT_MODE_2N, TVHT_MODE_4C or TVHT_MODE_4N (2x or 4x BCU)
- Two or more spatial streams (for transmission and reception)
- Beamforming sounding (by transmitting VHT NDP (Null Data Packet) frame)
- Response to beamforming sounding transmission (providing compressed beamforming feedback)
- STBC (for transmission and reception)
- LDPC (Low-Density Parity-Check) for transmission and reception
- VHT MU PPDUs (Physical Layer Protocol Data Unit) (for transmission and reception)
- MCSs 8 and 9 (for transmission and reception)

2.1 802.11af PHY scheme

The basic model of the transmitter block diagram is shown in Fig 2.2. In the first block are generated input data with a defined length. Such generated input data are structured into the PPDU frame according to the IEEE 802.11af standard. The next block is a data scrambler. On the output of the scrambler, the data input has a pseudo-random character. Further, the FEC (Forward Error Correction) encoder performs data encoding. To achieve the required coding rate is used the convolutional encoder with puncturing. In the next block, the encoded data are interleaved to minimize symbol error during transmission. Further, the demultiplexed serial data bit stream is modulated by the subcarriers modulation defined in the IEEE

802.11af standard. Also, the pilot subcarriers mapping is performed. After subcarriers mapping is performed the IFFT (Inverse Fast Fourier Transform) conversion into the time domain. Into transformed signal is inserted cyclic prefix. As a result, the signal is prepared for RF (Radio Frequency) processing to the next transmission in the communication channel [2],[7].

The mode SISO (Single-Input Single-Output) describes the configuration of the communication system which contains one antenna for each the transmitter and receiver. Such a communication system does not require space diversity. One of the main advantages of that system is a simple implementation [9].

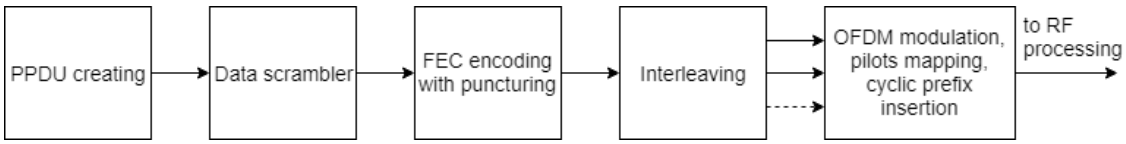

Fig. 2.2: Transmitter block diagram (based on [7]).

In the next description of the transmitter model is considered non-HT (Non High Throughput) duplicate mode. In addition, the next description covers the different between non-HT duplicate and VHT modes. For that description is used SISO mode with one spatial stream. Basic, the TVHT system uses orthogonal frequency division multiplex. The data transmission rate for each PSDU (Physical Layer Service Data Unit) in the system can reach 6, 9, 12, 18, 24, 36, 48, and 54 Mbit/s divided by X. The variable X is a constant defined by regulatory authority. For channel bandwidths, 6 MHz and 7 MHz variable X equals to 7.5. Otherwise, for 8 MHz channel variable X equals 5.625. For example, the maximum data rate for 6 MHz and 7 MHz channels is calculated as $\frac{54}{7.5} = 7.2Mbit/s$ and for 8 MHz channel is calculated as $\frac{54}{5.625} = 9.6Mbit/s$[7].

The system contains 104 subcarriers including pilots per one BCU. Each subcarrier can be modulated with BPSK, QPSK, 16QAM, and 64QAM modulations. The system parameters depending on the chosen modulation are represented in Tab. 2.1. In the channel coding are used coding rates R=1/2, R=2/3, or R=3/4. For example, to achieve the maximum data rate according to Tab. 2.2 is necessary to choose modulation 64QAM, R=3/4, $N_{BPSC} = 6$ and $N_{CBPS} = 288$ [7].

Tab. 2.1: Modulation-dependent parameters for Non-HT duplicate mode [7].

Modulation	**Coding rate** (R)	**Coded bits per subcarrier** (N_{BPSC})	**Coded bits per OFDM symbol** (N_{CBPS})	**Data bits per OFDM symbol** (N_{DBPS})	**Data rate (Mbit/s) (TVWS band)**
BPSK	1/2	1	48	24	6/X
BPSK	3/4	1	48	36	9/X
QPSK	1/2	2	96	48	12/X
QPSK	3/4	2	96	72	18/X
16QAM	1/2	4	192	96	24/X
16QAM	3/4	4	192	144	36/X
64QAM	2/3	6	288	192	48/X
64QAM	3/4	6	288	216	54/X
X = 7.5 for 6 MHz and 7 MHz unit channels and X = 5.625 for 8 MHz channels.					

The time parameters for Non-HT PDDU are mentioned in Tab. 2.2. It contains two types of cyclic prefixes: normal and short. The normal cyclic prefix is two times longer than the short one. Moreover, the cycle prefix depends on the channel bandwidth used. The prefix is inserted in the OFDM modulation block according to Fig 2.2. The frequency subcarrier spacing is calculated as the ratio of channel bandwidth to the number of subcarriers. For example, when 8 MHz channel is used the number of subcarriers is equal to 144. Consequently, the frequency subcarrier spacing is calculated as $\frac{8MHz}{144} = 55\frac{5}{9}kHz$ [7].

Tab. 2.2: Timing-related constants in Non-HT PPDU [7].

Parameter	**6 MHz**	**7 MHz**	**8 MHz**	**Description**
N_{SD}	96	96	96	Number of complex data numbers per BCU
N_{SP}	8	8	8	Number of pilot values per BCU
N_{ST}	104	104	104	Total number of subcarriers per BCU
N_{SR}	58	58	58	Highest data subcarrier index per BCU
Δf	$41\frac{2}{3}kHz$	$41\frac{2}{3}kHz$	$55\frac{5}{9}kHz$	Subcarrier frequency spacing
T_{DFT}	$24\mu s$	$24\mu s$	$18\mu s$	IDFT/DFT period
T_{GI}	$6\mu s = \frac{T_{DFT}}{4}$	$6\mu s = \frac{T_{DFT}}{4}$	$4.5\mu s = \frac{T_{DFT}}{4}$	Guard interval duration
T_{GIS}	$3\mu s = \frac{T_{DFT}}{8}$	$3\mu s = \frac{T_{DFT}}{8}$	$2.25\mu s = \frac{T_{DFT}}{8}$	Short guard interval duration

For the VHT mode, the number of complex data number per BCU $N_{SD} = 108$ and the number of pilot values per BCU $N_{SP} = 6$. As a result, the total number of subcarriers per BCU $N_{ST} = 114$. All differences in time-related constants for VHT PPDU are shown in Appendix A.1. Moreover, the VHT mode is extended for using 256-QAM modulation and coding rate 5/6. All permitted modulation-dependent parameters are shown in Appendix A.2. [7].

2.2 PPDU format

The PDDU format according to Fig. 2.3 contains the OFDM PHY preamble, the OFDM PHY header, PSDU, the tail bits and pad bits. The PHY header is consist of the LENGTH, the RATE, a reserved bit, an odd parity bit and the SERVICE field. In the modulation part, one OFDM symbol consisting of the fields LENGTH, RATE, a reserved bit and parity bit together with six tail bits forms the SIGNAL field. This field is transmitted with a more robust combination of the BPSK modulation and the coding rate R=1/2 [7].

The fields SERVICE, PSDU, six tail bits and pad bits are considered to be the DATA field. Such DATA fields are transmitted with coding rate described in the RATE field and it can represent a few OFDM symbols. In conclusion, the PPDU contains three fields: the PHY preamble, the SIGNAL, and the DATA [7].

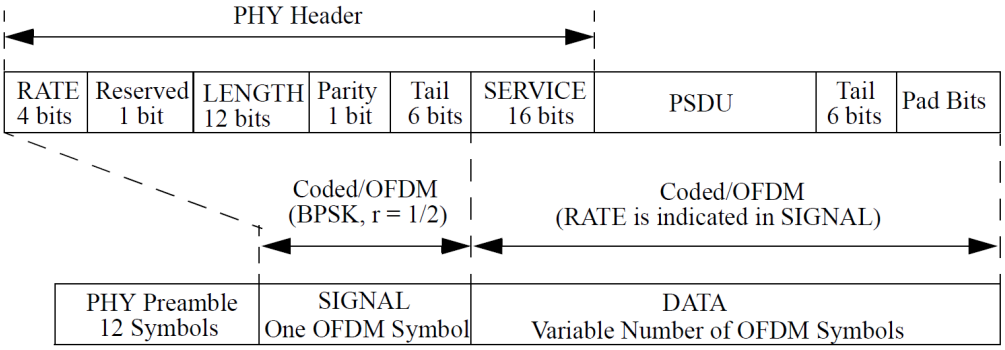

Fig. 2.3: PPDU format [7].

The PHY preamble field is used for synchronization. It consists of 10 short and two long symbols. In the case of the 20 MHz channel, the full training length have 16 μs [7].

According to Fig 2.4, the field SIGNAL is consists of the field RATE, a reserved bit, the LENGTH, parity bit, the TAIL bits which together take 24 bits length. The SIGNAL part has one OFDM symbol length, and it is always BPSK modulated with coding rate R=1/2. Moreover, the SIGNAL part is not scrambled. The RATE field is defined with 4 bits from R1 to R4 which transmits information about the type of modulation and coding rate used in the rest of the packet. Bit 4 is considered as reserved. The bits from 5 to 16 define 12 bits unsigned number. This number indicates a number of octets transmitted in the PSDU. The first is transmitted bit 5 LSB. The last is the transmitted bit 16 MSB. The parity bit 17 has to be a positive parity for the bits from 0 to 16. The bits from 18 to 23 are set on the value "0" [7].

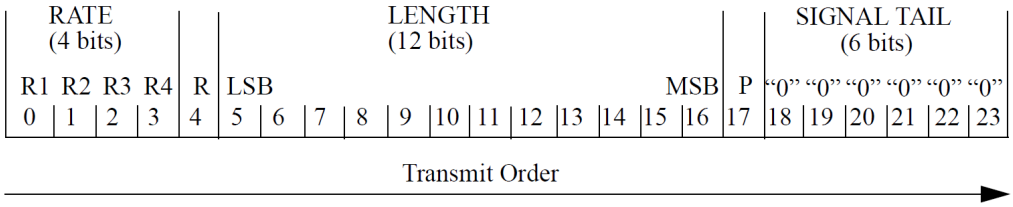

Fig. 2.4: SIGNAL field bit assignment [7].

For the non-HT duplicate PPDU format is permitted 4095 bytes maximum length of the PSDU. For the VHT PPDU format is considered only DATA part of the PPDU. In such PPDU format is permitted 1 065 600 bytes maximum length of the PSDU. [7].

2.3 Scrambler

Basically, the scrambler is a block to perform data scrambling when data are converted without speed rate changes. A sequence has pseudo-random properties after data scrambling applied. The long sequences with zeros and ones are spread [7].

For the data part of the IEEE 802.11 frame have to be applied the PPDU synchronous scrambler with the length 127 bits. The generator polynomial S(x) according to the equation 2.1 is used in the PDDU synchronous scrambler [7]. The data scrambler schematically can have the form regarding Fig. 2.5 [7].

In the data scrambler are defined initialization sequence on the seven first bits with ones. The bit sequence is processed from LSB right to MSB left [7].

$$S(x) = x^7 + x^4 + 1 \tag{2.1}$$

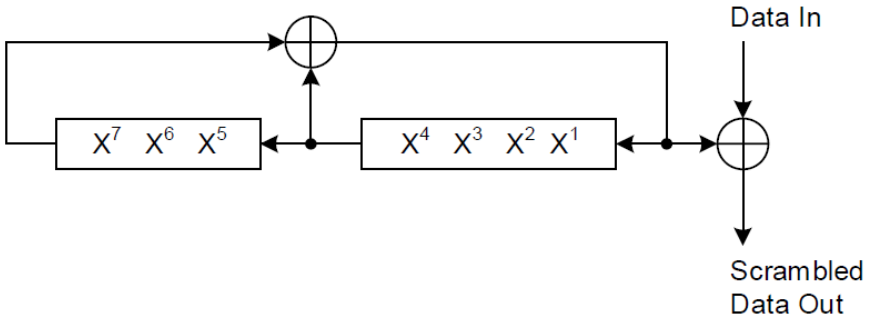

Fig. 2.5: Data scrambler [7].

2.4 Convolutional encoder

In the IEEE 802.11 standard for the channel coding of the data frame is used the convolutional encoder with the coding rates $R = 1/2$, $2/3$ or $3/4$. The convolutional encoder uses the generator polynomial's coefficients $G_0 = 133$ a $G_1 = 171$ in an octal number system with the rate $R = 1/2$. The bit stream is formed by two output branches according to Fig. 2.6. It is processed sequentially as the bit A and bit B. The remaining coding rates are derived from the procedure, which is called the puncturing. The puncturing omits some coding bits in the transmitter. Therefore, on the convolutional decoder are inserted the fictitious zeros instead of such omitted

bits. The example of puncturing in the convolutional data encoder and decoder for the coding rate $R = 3/4$ is mentioned in Fig. 2.7 [7][10].

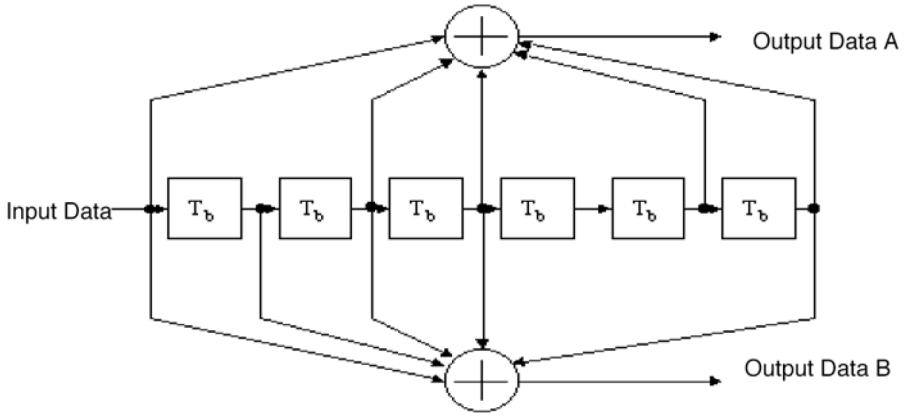

Fig. 2.6: Convolutional encoder [7].

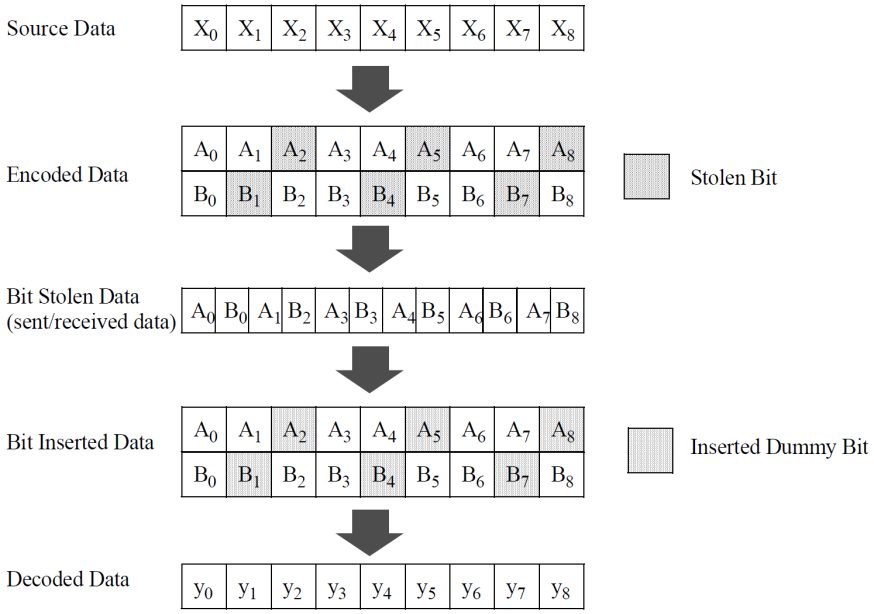

Fig. 2.7: Example of the bit-stealing and bit-insertion procedure for the coding rate $R = 3/4$ [7].

For the VHT format is used the same convolutional encoder. Moreover, in such format is allowed puncturing with the coding rate $R = 5/6$. [7].

2.5 LDPC encoder

In this master thesis is considered binary convolutional encoder, which is described in the part 2.4. Also, in the IEEE 802.11af standard is not prohibited from using LDPC encoder. Such expansion provides to reach better error correction in comparison with the convolutional encoder usage. The LDPC encoder is related to the block encoder, which is different from the convolutional encoder. The choice of the LDPC block encoder is connected with a coding rate of such encoder. The length of an information block and the coding block of LDPC codes are fixed [12].

2.6 Interleaving

All coded data bits are interleaved with a block size corresponding to a number of bits per one OFDM symbol N_{CBPS}. The interleaving is defined by two steps permutation. The first permutation is focused on the mapping of the adjusted coding bits into the non-adjacent subcarriers. The second permutation is focused on the mapping of the adjusted coding bits, which have to be mapped alternately into the least and most significant bits of the constellation. As a result, the continually sequences with the LSB (Least Significant Bit) bits are prevented [7].

The index of the coding bits before the first permutation is defined as k. The index for the first and second permutations are defined as i. The index after the second permutation is defined as j [7].

The first permutation is defined according to the rule in equation 2.2 [7]. The second permutation is defined according to the rule in equation 2.3 [7]. The value s is defined by the number of the coding bits per subcarrier N_{BPSC} according to the equation 2.4 [7].

$$i = (N_{CBPS}/16) \times 2(k \bmod 16) + \lfloor k/16 \rfloor, k = 0, 1, ..., N_{CBPS} - 1 \tag{2.2}$$

$$i = s \times \left\lfloor \frac{i}{s} \right\rfloor + \left(i + N_{CBPS} - \left\lfloor \frac{16 \times i}{N_{CBPS}} \right\rfloor \right) \bmod s, i = 0, 1, ..., N_{CBPS} - 1 \tag{2.3}$$

$$s = \max(\frac{N_{BPSC}}{2}, 1) \tag{2.4}$$

For the VHT PPDU format are defined the number of columns N_{COL} and the number of rows N_{ROW} used in the interleaver according to appendix A.3. In such format are used two permutation rules described in appendix A.4 and A.5. [7].

2.7 OFDM modulation

In the IEEE 802.11af standard is used the OFDM modulation to produce the OFDM symbols in the transmitting channel. OFDM is a form of frequency division multiplexing in which a single channel utilizes multiple subcarriers on adjacent frequencies. Subcarriers in an OFDM system are precisely orthogonal to one another. It allows subcarriers to be overlapped without interfering. The orthogonality of the OFDM system is caused by sinc-shaped pulses applied in the frequency domain of each channel as shown in Fig. 2.8 [21].

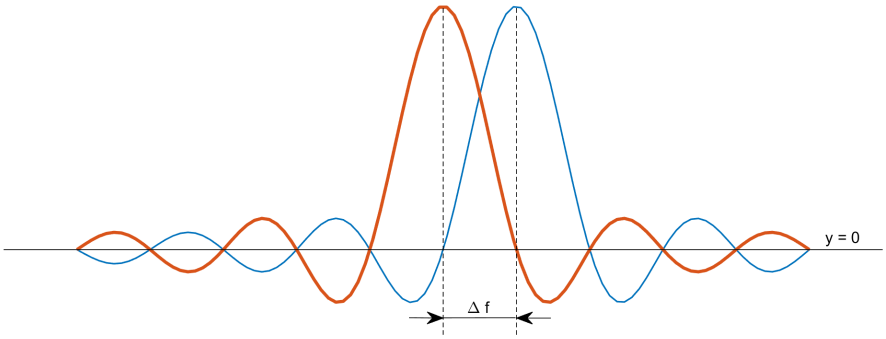

Fig. 2.8: OFDM symbols orthogonality (based on [21]).

The subcarrier frequency spacing is defined as Δf between each subcarriers per single channel [21].

The next blocks in the transmitter are focused on the OFDM symbols creation according to Fig. 2.9. At the beginning in the modulator block is performed the PSK (Phase Key Shifting) or the QAM (Quadrature Amplitude Modulation) modulation. Next, the modulated symbols are divided into the parallel streams with the S/P (Serial to Parallel Converter) converter. Such divided streams are mapped into the IFFT block inputs. In the next IFFT block is performed the transformation of symbols from frequency to the time domain. Moreover, in the frequency domain are inserted the pilot subcarriers. After that, the parallel streams are converted into a sequence of symbols using the P/S (Parallel to Serial Converter). To each symbol in the time domain is added a cyclic prefix to suppress the ISI (Inter-Symbol Interference). As a result, the OFDM symbols are produced on the output, which are prepared for the next processing in the transmission channel [11].

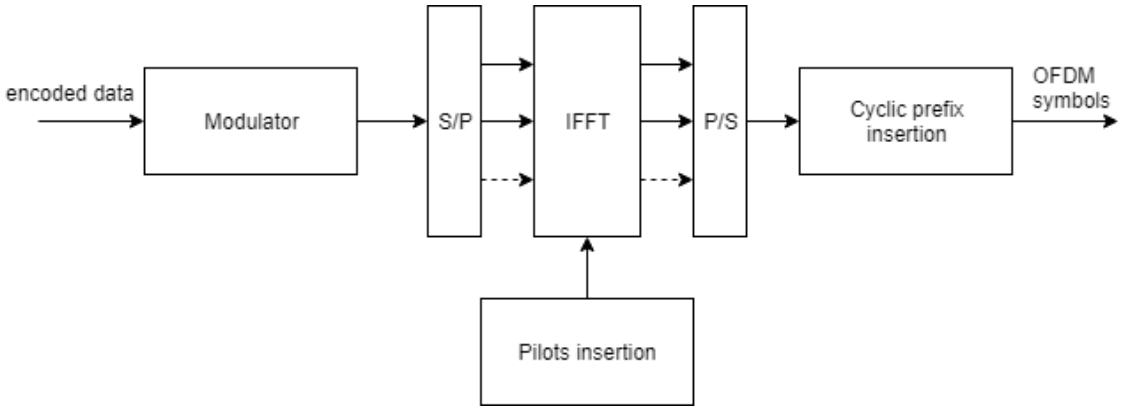

Fig. 2.9: OFDM modulator (based on [11]).

2.7.1 Subcarrier modulation

In the standard IEEE 802.11, the OFDM symbols are modulated BPSK, QPSK, 16QAM or 64QAM depending on the system configuration selected. The coded and interleaved binary serial input data are divided into groups of the N_{BPSC} (1, 2, 4 or 6) bits and converted to the symbols given by the constellation of the BPSK, QPSK, 16QAM or 64QAM modulation [7]. The conversion into symbols is performed with the Gray coding basis according to Fig. 2.10. The output values "d" are formed with the In-phase (I) and Quadrature (Q) axes. The resulted $(I + jQ)$ symbols are multiplied by the normalization factor K_{MOD} according to equation 2.5 [7].

$$d = (I + jQ) \times K_{MOD} \tag{2.5}$$

The normalization factor K_{MOD} value based on the type of the modulation used regarding the table in Tab. 2.3. It is important to note that the normalization factor K_{MOD} gives the opportunity to gain the same average power for each mapping. In a practical implementation, the approximate value of the normalization factor can be used when equipment meets the requirements on the modulation precise [7].

Tab. 2.3: Modulation-dependent normalization factor K_{MOD} [7].

Modulation	K_{MOD}
BPSK	1
QPSK	$\frac{1}{\sqrt{2}}$
16QAM	$\frac{1}{\sqrt{10}}$
64QAM	$\frac{1}{\sqrt{42}}$

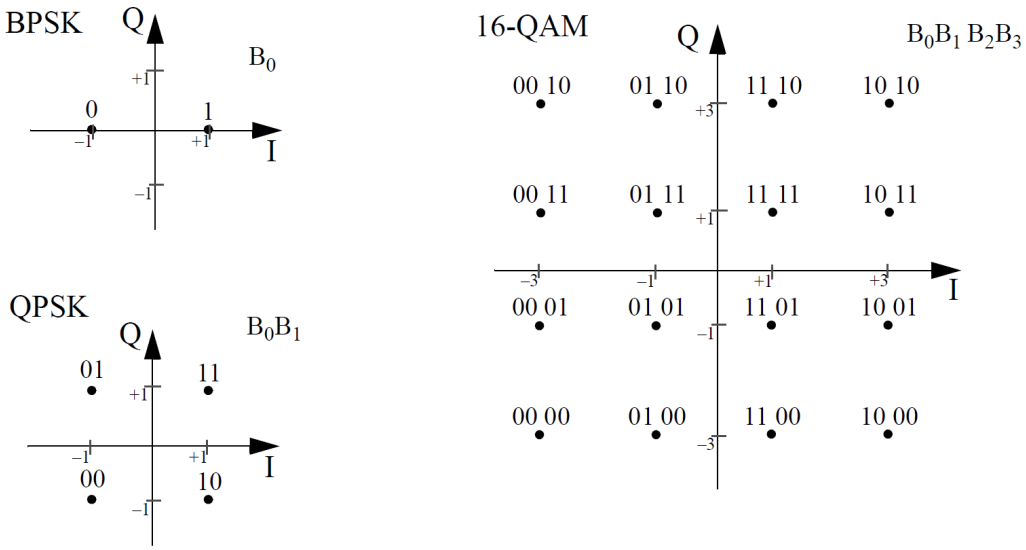

Fig. 2.10: BPSK, QPSK, and 16-QAM constellation bit encoding [7].

In the VHT format of the PPDU can also be used 256-QAM modulation where the number of coded bits per subcarrier $N_{BPSC} = 8$. In that case the normalization factor $K_{MOD} = \frac{1}{\sqrt{170}}$. [7].

2.7.2 Pilot subcarriers

In each OFDM symbol are subcarriers related to the pilot signals. The pilot signals are the BPSK modulated. It is used for the coherent robustness detection against frequency shifts and phase noise. For the non-HT duplicate format of PPDU are allocated 8 such pilots on subcarrier indexes -53, -39, -25, -11, 11, 25, 39, 53 in the mandatory TVHT_MODE_1 configuration. For each channel configuration in the non-HT duplicate format with BCU 6 and 8 MHz are described the pilots mapping in Tab. 2.4. For each channel configuration in the same format with BCU 7 MHz are described the pilots mapping in Tab. 2.5. The sign of pilot values is defined according to the output sequence of the scrambler, which is described in 2.3 [7].

In the VHT format of PPDU are allocated 6 pilots on subcarrier indexes -53, -25, -11, 11, 25, 53 in the mandatory TVHT_MODE_1 configuration. For each channel configuration in the VHT format with BCU 6 and 8 MHz are described the pilots mapping in appendix A.6. For each channel configuration in the same format with BCU 7 MHz are described the pilots mapping in appendix A.7 [7].

Besides, the subcarrier with index 0 is called the DC, which does not carry any useful data [7].

Tab. 2.4: Pilots mapping for BCU 6 and 8 MHz [7].

Channel configuration	Pilot indexes
TVHT_MODE_1	{-53,-39,-25,-11,11,25,39,53}
TVHT_MODE_2C	{-125,-111,-97,-83,-61,-47,-33,-19,19,33,47,61,83,97,111,125}
TVHT_MODE_2N	{-53,-39,-25,-11,11,25,39,53} for each BCU
TVHT_MODE_4C	{-269,-255,-241,-227,-205,-191,-177,-163,-125,-111, -97,-83,-61,-47,-33,-19,19,33,47,61,83,97,111, 125,163,177,191,205,227,241,255,269}
TVHT_MODE_4N	{-125,-111,-97,-83,-61,-47,-33,-19,19,33,47,61,83,97,111,125} for each BCU

Tab. 2.5: Pilots mapping for BCU 7 MHz [7].

Channel configuration	Pilot indexes
TVHT_MODE_1	{-53,-39,-25,-11,11,25,39,53}
TVHT_MODE_2C	{-137,-123,-109,-95,-73,-59,-45,-31,31,45,59,73,95,109,123,137}
TVHT_MODE_2N	{-53,-39,-25,-11,11,25,39,53} for each BCU
TVHT_MODE_4C	{-305,-291,-277,-263,-241,-227,-213,-199,-137,-123, -109,-95,-73,-59,-45,-31,31,45,59,73,95,109,123, 137,199,213,227,241,263,277,291,305}
TVHT_MODE_4N	{-137,-123,-109,-95,-73,-59,-45,-31,31,45,59,73,95,109,123,137} for each BCU

2.7.3 Creating OFDM symbols

The OFDM modulation process was shown in Fig. 2.9. A stream of modulated subcarriers is divided into groups of data subcarriers N_{SD} defined according to Tab. 2.2. [7].

For the example will be considered OFDM symbol creation in the basic channel configuration TVHT_MODE_1 for all BCU defined by the IEEE 802.11af standard. The number of data subcarriers $N_{SD} = 96$. The data mapping for each channel configuration is defined in Tab. 2.6 for BCU 6 and 8 MHz and Tab. 2.7 for BCU 7 MHz. For the channel configuration TVHT_MODE_1, subcarrier frequency allocation of the FFT block is shown in Fig. 2.11. The data subcarriers are allocated on the indexes -58 to -33, -31 to -6, 6 to 31, and 33 to 58 as shown in Fig. 2.11. Eight of these subcarriers are related to pilots which are marked as red in Fig. 2.11. The minimal FFT block size for that channel configuration is chosen as 128 subcarriers. As a result, remain subcarriers are nulls which are marked as gray in Fig. 2.11 and

their number is calculated as $FFT\_size - N_{ST}$ what gives $128 - 104 = 24$ nulls. [7].

The frequency spacing for the previously described example is $55\frac{5}{9}kHz$ for BCU 8 MHz and $41\frac{2}{3}kHz$ for BCU 6 and 7 MHz. In the time domain, the duration of created FFT block is $18\mu s$ for BCU 8 MHz and $24\mu s$ for BCU 6 and 7 MHz. To such FFT block is added normal cyclic prefix with duration for $4.5\mu s$ for BCU 8 MHz and $6\mu s$ for BCU 6 and 7 MHz. As a result, the duration of the created OFDM symbol is calculated as $T_{DFT} + T_{GI}$ what gives $22.5\mu s$ for BCU 8 MHz and $30\mu s$ for BCU 6 and 7 MHz [7].

Tab. 2.6: Data mapping for BCU 6 and 8 MHz [7].

Channel configuration	Data indexes
TVHT_MODE_1	-58 : -33, -31 : -6, 6 : 31, 33 : 58
TVHT_MODE_2C	-130 : -105, -103 : -78, -66 : -41, -39 : -14, 14 : 39, 41 : 66, 78 : 103, 105 : 130
TVHT_MODE_2N	-58 : -33, -31 : -6, 6 : 31, 33 : 58 for each BCU
TVHT_MODE_4C	-274 : -249, -247 : -222, -210 : -185, -183 : -158, -130 : -105, -103 : -78, -66 : -41, -39 : -14, 14 : 39, 41 : 66, 78 : 103, 105 : 130, 158 : 183, 185 : 210, 222 : 247, 249 : 274
TVHT_MODE_4N	-130 : -105, -103 : -78, -66 : -41, -39 : -14, 14 : 39, 41 : 66, 78 : 103, 105 : 130 for each BCU

Tab. 2.7: Data mapping for BCU 7 MHz [7].

Channel configuration	Data indexes
TVHT_MODE_1	-58 : -33, -31 : -6, 6 : 31, 33 : 58
TVHT_MODE_2C	-142 : -117, -115 : -90, -78 : -53, -51 : -26, 26 : 51, 53 : 78, 90 : 115, 117 : 142
TVHT_MODE_2N	-58 : -33, -31 : -6, 6 : 31, 33 : 58 for each BCU
TVHT_MODE_4C	-310 : -285, -283 : -258, -246 : -221, -219 : -194, -142 : -117, -115 : -90, -78 : -53, -51 : -26, 26 : 51, 53 : 78, 90 : 115, 117 : 142, 194 : 219, 221 : 246, 258 : 283, 285 : 310
TVHT_MODE_4N	-142 : -117, -115 : -90, -78 : -53, -51 : -26, 26 : 51, 53 : 78, 90 : 115, 117 : 142 for each BCU

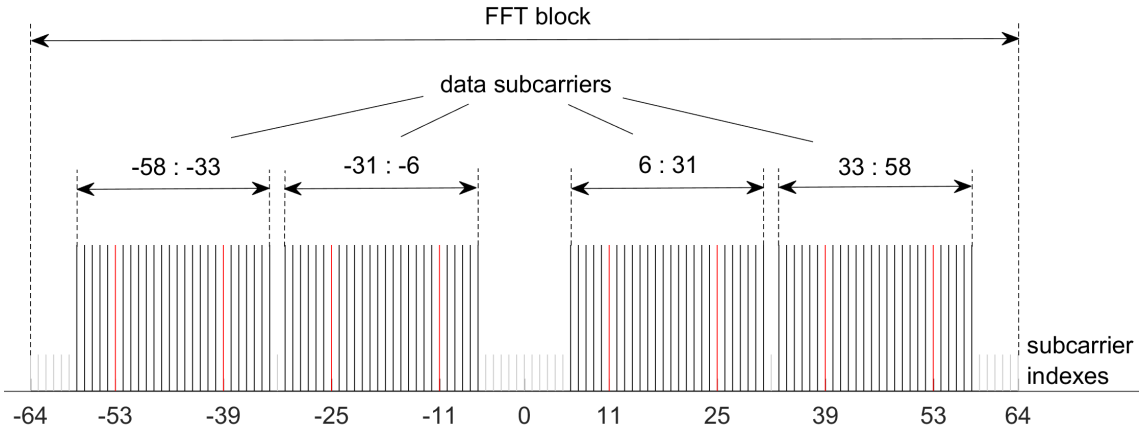

Fig. 2.11: Subcarrier frequency allocation (based on [7]).

For each channel configuration in the VHT format with BCU 6 and 8 MHz are described the data subcarriers mapping in appendix A.8. For each channel configuration in the same format with BCU 7 MHz are described the pilots mapping in appendix A.9 [7].

2.8 MIMO

Previously described parts of the communication channel containing the transmitter and receiver are defined for the SISO mode. In such mode are considered one transmitting and one receiving antennas. Moreover, the IEEE 802.11af standard allows using another mode, which is called the MIMO mode. It is a commonly used mode, which uses more than one antenna on both transmitter and receiver sides [13].

To reach more robust radio communication are used different types of diversity. The first one is the time diversity, which uses different time slots and channel coding. The second one is the frequency diversity, which uses different channels as in the case of the OFDM. The last one is space diversity, which requires using multiple antennas in the transmitter and receiver [13]. Actually, the MIMO mode uses the multipath signal propagation in free space. As a result, using more than one antenna makes the transmission data rate higher. Moreover, the error rate during transmission is reduced [13].

Basically, the MIMO system consists of N_t transmitting and N_r receiving antennas according to Fig. 2.12. Each antenna using one channel can receive signals from multiple antennas. The direct transmission between first transmitting and second receiving antennas is defined by channel coefficient $h_{1,1}$. For example, the indirect

transmission between first transmitting and second receiving antennas is defined by $h_{2,1}$. The whole transmission of the MIMO system is described by the matrix according to equation 2.6 [13].

$$H = \begin{pmatrix} h_{1,1} & h_{1,2} & \cdots & h_{1,N_t} \\ h_{2,1} & h_{2,2} & \cdots & h_{2,N_t} \\ \vdots & \vdots & \ddots & \vdots \\ h_{N_r,1} & h_{N_r,2} & \cdots & h_{N_r,N_t} \end{pmatrix} \tag{2.6}$$

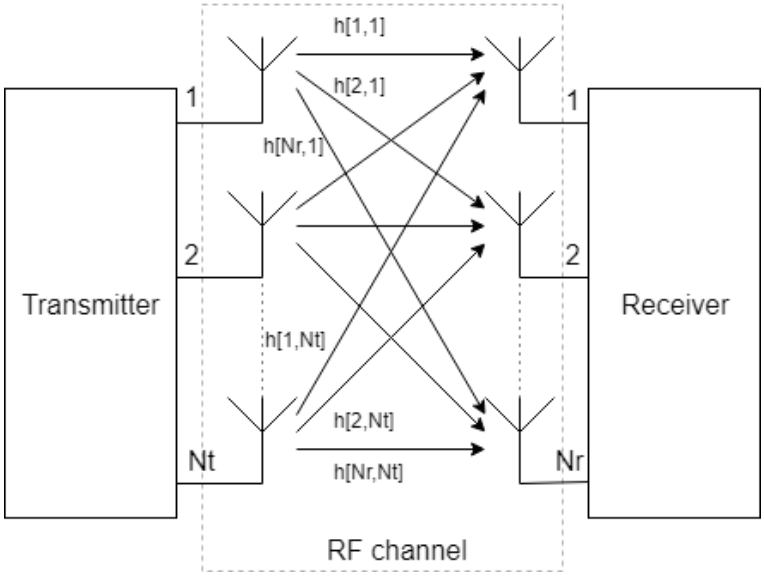

Fig. 2.12: MIMO system scheme (based on [13]).

In the IEEE 802.11af standard is supported system configuration MIMO with up to 4 transmitting and 4 receiving antennas. In the current thesis will be considered basic system configuration MIMO 2x2. In such configuration, space diversity is formed by 2 transmitting and 2 receiving antennas according to Fig. 2.13. Channel matrix for such configuration is defined by the equation 2.7. One of the advantages in such configuration is double data throughput in comparison with SISO. Moreover, it helps in achieving a reduction in the BER of the transmission and also it minimizes the fading effect in the multipath propagation. [13]

$$H = \begin{pmatrix} h_{1,1} & h_{1,2} \\ h_{2,1} & h_{2,2} \end{pmatrix} \tag{2.7}$$

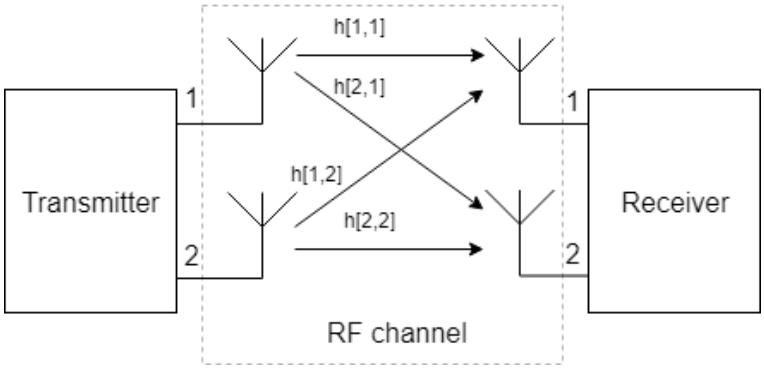

Fig. 2.13: MIMO 2x2 system scheme (based on [13]).

In the MIMO system are concerned the SU-MIMO (Single-User Multiple-Input-Multiple-Output) and the MU-MIMO (Multi-User Multiple-Input-Multiple-Output) modes. In the case of the SU-MIMO, the communication is processed with each user. It is mainly used to gain data rate for the selected receiver. In the case of MU-MIMO communication, each data stream is assigned to multiple users. Such mode is especially used for the uplink with one transmitting antenna. The complexity of the receiver is minimal for this configuration [13].

The capacity for a MIMO system is defined with the number of data streams M by equation 2.8. The M value is related to a minimum or less than the minimum number of antennas in a MIMO system. For example, in the MIMO 4x4 system, data can be transmitted by four or less M data streams. In the case of the MIMO 3x2 system, data can be transmitted by two or less M data streams [13].

$$C = M * B * log_2\left(1 + \frac{S}{N}\right) \tag{2.8}$$

, where M is the number of data streams, B is the channel bandwidth, S is the level of a desired signal and N is the noise level in a channel [13].

2.8.1 Space-Time Block Codes (STBC)

In the MIMO system, the data stream is basically divided, coded, and modulated. After the modulation is used the STBC coding block as on the transmitter and receiver sides [14].

The STBC codes are orthogonal and form space and time diversity defined by the number of transmitting antennas. One of the implementations of STBC codes is the Alamouti scheme. The Alamouti scheme of coding and decoding are the same on the receiver and transmitter. The data are created with a matrix. Columns of such matrix are related to the number of transmitting antennas. Rows of such

matrix are related to the number of time slots of zeros to transmit the data. The received signals in the receiver are combined and then transmitted to the maximum likelihood detector whether process decision-making. The STBC is designed to gain maximum order of diversity for the defined number of transmitting and receiving antennas. In terms of reception, the STBC is quite popular and widely used due to the low computing complexity. Such a block is necessary for the MIMO systems and can be part of the system defined by the IEEE 802.11af standard [14].

The STBC allows transmitting multiple copies of the data stream throughout the multiple antennas. As a result, several versions of the data stream are received. Such an approach increases the reliability of data transmission. The STBC coding combines each copy of the received signal in an optimal way to gain a maximum of useful information from each signal. The problem with a channel as the attenuation and thermal noise is compensated by transmitting multiple copies of the data stream. Through the data stream redundancy is improved quality of the reception [14].

Basically, the STBC block is defined with matrix S. As previously described each row represents the time slot and each column represents transmission by one antenna per the time slot. Each modulated symbol of the matrix $S_{ij}j$ is transmitted in the time slot i from antenna j. Have to be T time slots, nT transmitting antennas, and nRreceiving antennas. Such block is usually defined by length T [14].

The transmission matrix S for two transmitting antennas implemented with Alamouti scheme is defined by equation 2.9. One of the advantages is that STBC coding does not require knowledge of channel characteristic [14].

$$S = \begin{pmatrix} s_1 & s_2 \\ -s_2^* & s_1^* \end{pmatrix} \tag{2.9}$$

2.8.2 Cyclic Shift Diversity (CSD)

In the IEEE 802.11af standard, the OFDM modulator for the high throughput channel is extended by the CSD block. The main function for such block is focused on preventing unintentional creation of the transmitting beam. In the case of the CSD, the signals are transmitted by the individual antennas with the time delay. Consequently, the frequency selectivity on the receiver is increased. In addition, the CSD introduces the next diversity component whether is especially useful as a component to spatial multiplexing. Basically, the CSD block is assigned in the transmitter after the inverse Fourier Transform process. The different allocation of the CSD block can be after the STBC block [12].

2.9 Channel transmission models

The IEEE 802.11af communication system is based on wireless data transmission. Between the transmitter and receiver can be found the communication channel consisting of the free space and obstacles. Through such channel are transmitted the data created by the transmitting part described in chapter 2. In the real antenna transmission occurs phenomena such as free space losses, refraction, diffraction, reflection an absorption by obstacles. All of such phenomena affect losses of the transmitting signal by the communication channel. In this part are described the mathematical communication channel models which are based on such phenomena. Such models are also called fading channels [15].

2.9.1 Additive White Gaussian Noise (AWGN) channel

The AWGN channel is the simplest channel model. Such a channel is based on additive white Gaussian noise. This noise is basically thermal noise. In wireless communications such noise is produced by atoms vibrations in electronics on a receiver. This model is represented by the sum of the transmitting signal and AWGN noise according to equation 2.10 and Fig. 2.14. It means that on the receiver is occurred such sum. The spectral power for such noise is the same on the whole frequency band. In the time domain, the probability occurrence of noise values is defined by the Gaussian distribution. Thus, the probability occurrence of noise close to zero is the greatest [16].

$$y[k] = x[k] + n[k] \tag{2.10}$$

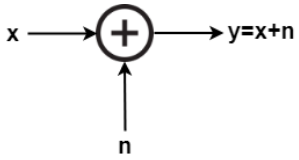

Fig. 2.14: AWGN channel (based on [16]).

2.9.2 Rician channel

The real communication channel much more difficult on a type of leakages. In the previous model was considered only the AWGN noise. Often the signal or signals between the transmitter and receiver are multipath propagated. It means that exists the high probability for the signal reflections by the obstacles. For each

signal location of reflection at most differs. It has appeared in the delay and phase changes of each signal. The same is valid for the amplitude of the received signals. Moreover, in the mobile communications are often the receiver moved in time. It leads to a Doppler shift. Such reflections are included in the Rician transmission model. In such a model, the received signals in the line of sight are dominated over the individual reflections by the obstacles. The output signal $y(t)$ in the Rician model is defined by the equation 2.11 [15].

$$y(t) = \frac{\rho_0 * x(t) + \sum_{i=1}^{N_e} \rho_i * e^{-j2\pi\theta_i} * x(t - t_i)}{\sqrt{\sum_{i=0}^{N_e} \rho_i^2}} \tag{2.11}$$

, where ρ_0 is the attenuation in the line of sight, N_e is the number of the reflected signals, ρ_i is the attenuation on the reflection path, θ_i is the phase rotation on the reflection path i and t_i is the relative delay on the reflection path i. The Rician factor K defines the signal in the line of sight to the sum of all reflected signals ratio according to equation 2.12 [15].

$$K = \frac{\rho_0^2}{\sum_{i=0}^{N_e} \rho_i^2} \tag{2.12}$$

The parameters for RC and RA channel models are defined in Tab. 2.8, where ρ is the attenuation of the path i, τ is the relative delay of the path i and θ is the phase shift from the scattering of the path i.

Tab. 2.8: Fading parameters for RC12 and RA12 channel models [7].

path i	$\rho[-]$	$\tau[\mu s]$	$\theta[rad]$
1	0.407163	0.518650	5.864470
2	0.303585	2.751772	2.215894
3	0.258782	0.602895	3.758058
4	0.185074	3.324866	5.775198
5	0.400967	1.935570	0.154459
6	0.295723	0.429948	5.928383
7	0.350825	3.228872	3.053023
8	0.262909	0.848831	0.628578
9	0.225894	0.073883	2.128544
10	0.240140	0.924450	3.664773
11	0.221155	0.640512	3.334290
12	0.259730	1.368671	0.393889

2.9.3 Rayleigh channel

In the case of the signal is scattered between the transmitter and receiver is used the Rayleigh model. Such a model is more applicable if not any dominant signal is presented. In the case of the Rician factor $K = 0dB$, the signal in the line of sight is excluded. As a result, the whole Rayleigh channel is defined by the equation 2.13 [15],[17].

$$y(t) = \frac{\sum_{i=1}^{N_e} \rho_i * e^{-j2\pi\theta_i} * x(t - t_i)}{\sqrt{\sum_{i=0}^{N_e} \rho_i^2}} \tag{2.13}$$

2.9.4 Pedestrian Indoor channel

To simulate slowly moving indoor reception (speed 3 km/h) is used PI (Pedestrian Indoor) channel model. The channel model consists of 12 independent paths, where the first path is direct. The first path has a Doppler spectrum with frequency-selective multipath Rician fading channel. Remain paths have Doppler spectrum with frequency-selective multipath Rayleigh fading channels.

The parameters for the PI channel model are defined in Tab. 2.9, where ρ is the attenuation of the path i and τ is the relative delay of the path i.

Tab. 2.9: Fading parameters for PI12 channel model [7].

path i	$\rho[-]$	$\tau[\mu s]$
1	1.000000	0.000000
2	0.478630	0.100000
3	0.301995	0.200000
4	0.223872	0.400000
5	0.216272	0.600000
6	0.206538	0.800000
7	0.154882	1.000000
8	0.173780	1.600000
9	0.179887	8.100000
10	0.154882	8.800000
11	0.278612	9.000000
12	0.275423	9.200000

2.10 Equalization

The received signal on the receiver is different from the output signal on the transmitter. One of the phenomena in the wireless channel is the occurrence of the

inter-symbol interference in the multipath propagation of the signal. For solving this problem is used the channel equalization which compensates the channel frequency distortion. By frequently used the channel equalization algorithms belongs the linear, ZF (Zero Forcing) and adaptive equalization. The purpose of equalization is the approximation of the distorted signal to the primary signal. Basically, the received signal by the equalizer can be defined as the product of transmitted signal and samples of the channel response with the added noise according to the equation 2.14 [11] [19] [20].

$$r_k = s_k \otimes c_k + n_k \tag{2.14}$$

2.10.1 Zero Forcing

In the Zero Forcing equalization is considered the inverse frequency channel response to a received signal according to Fig. 2.15. It is necessary for the signal recovery after passing through the channel. The ZF equalizer can remove the inter-symbol interference distortion in the absence of noise. In the real case, the ZF equalizer is mostly used when the inter-symbol interference distortion is considerably greater than the noise impact [11].

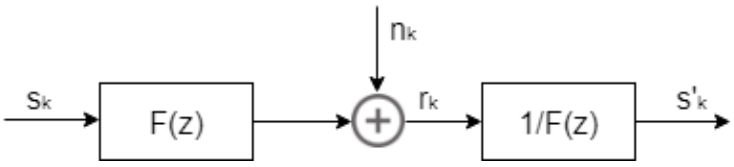

Fig. 2.15: Zero Forcing equalization [11].

The Zero Forcing equalization is based on the principle of the full channel inversion according to equation 2.15 [11].

$$c_k * g_k = \delta * (k - k_0) \tag{2.15}$$

The equivalent definition by the matrix can be used in equation 2.16 [11].

$$C * g = 1 \tag{2.16}$$

, where C is the square matrix of the discrete channel response samples and g is the column vector of the equalizer coefficients [11].

3 Program description

The components of the system defined by the IEEE 802.11af standard on the physical layer are described in chapter 2. Based on the description of these components the block diagram is designed for the transmitting and receiving parts of the IEEE 802.11af communication channel shown in Fig. 3.1. This model is implemented as a GUI application using the MATLAB programming environment according to Fig. 3.2 [18]. In this chapter, the implementation of each component and the application itself are described. Moreover, the procedures for the simulation handling and input model parameters setup are also defined in this chapter.

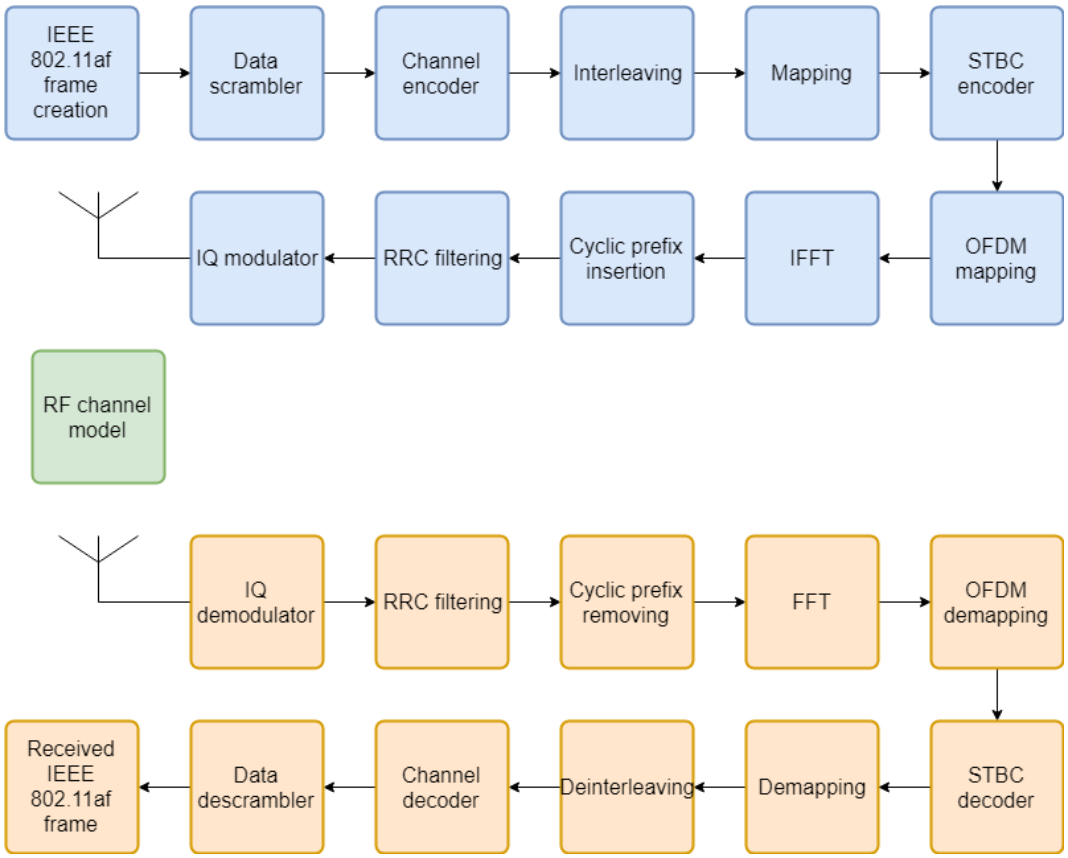

Fig. 3.1: Block diagram of the IEEE 802.11af communication model in MATLAB.

3.1 Block diagram model

In the presented block diagram shown in Fig. 3.1, the individual blocks are marked in different colors. First, blocks related to the transmitter are marked blue. Second, blocks related to the receiver are marked orange. Last, a model of the transmitting channel between blue and orange blocks is marked green.

3.2 Transmitter

3.2.1 Creating of IEEE 802.11af frame structure

In the transmitter, the first block is related to the frame generation defined by the IEEE 802.11af standard. Such a frame is fallen under the non-HT transmission which is supported in the IEEE 802.11af standard. The Non-HT frame contains the PDDU which is consisting of the SIGNAL and DATA fields according to 2.2. For each frame, the PSDU is measured in octets and can reach a maximum size of 4095 bytes. It is important to note that the frame has to be formed according to the IEEE 802.11af standard to gain success of processing throughout each communication block.

In the following description by the term of the internal function will be mentioned the function which is the part of MATLAB program environment. For the creating first part of the frame, the function `PPDU_SIGNAL` is used. Creating of this part is based on chosen parameters by a user as a length of input data and transmission rate. For the creating second part of the frame, `PSDU_generator` and `PPDU_DATA` functions are used. The pseudorandom data with defined length are created based on the user's length selection. The function uses the internal function `randi` with input value 255 which corresponds one data byte. Conversion to binary format is processed with the internal function `de2bi`. As a result, the output of the function `PSDU_generator` contains the pseudorandom sequence of the data bits. Such a sequence is the input of the function `PPDU_DATA`. This function creates a complete DATA field. It is created based on the SIGNAL field, modulation and coding scheme table which is defined in the program by the external file with the name MCS.txt. To conversion of data length from the binary format in the SIGNAL field to a decimal number is used the internal function `bi2de` which is part of the function `PPDU_DATA`. Moreover, to the conversion of the coding rate vector from the SIGNAL field to the string value is used the internal function `mat2str`. Last, to round value necessary for calculating the number of pad bits up is used the internal function `ceil`.

3.2.2 Data scrambling

The next block is related to the data scrambler which is used for the data part of the frame except for the SIGNAL field. The scrambler is implemented by the function `scrambler` with the input DATA field and initialization value s. The value s is equal to 127 to initialize the scrambler state starting with all ones. In the scrambler, the following internal functions are used: `bitxor` for bit operation xor between the 4th and 7th bits, `bitget` and `bitset` to read and set the corresponding bit, and `bitshift` to shift bit by one. An output of the function `scrambler` is binary

formed. It is implemented using the internal function `de2bi` with input parameters bit length of byte 8 and marking the most significant bit from the left. Then, the output of the scrambler is filled with mixed data using the inversion cycle for. The direction of the data flow output is the same as the input.

3.2.3 Data encoding

In the block of the channel coding, the binary convolutional encoder is implemented with the length equals 7. Each full frame is passed through the channel encoder. The coded data part of the frame is formed with the function `fec_coder` with the input mixed data and chosen coding rate. Remain coding part of the frame is formed with the same function with the input SIGNAL field and coding rate $R = \frac{1}{2}$. Moreover, the convolution encoder is implemented using the internal functions `poly2trellis` and `covenc`. The structure `trellis` is created with the first function. Forming the `trellis` structure is based on the length of the encoder which is equal to 7 and polynomial with coefficients $G_0 = 133$ and $G_1 = 177$. Finally, the convolutional coding with puncturing is processed by the function `convenc` using the trellis structure, input bits and coding data rate. As a result, the output number of the bits in the function `fec_coder` depends on the chosen coding data rate.

3.2.4 Data interleaving

The interleaving block is implemented by the function `interleaver`. The input coded bits are interleaved using the double permutation based on the chosen subcarriers modulation. Two parameters are defined in the chosen subcarriers modulation. First one is a number of the coding bits per the OFDM symbol. The second one is a number of the coding bits per the subcarrier. In the interleaver, the following internal functions are used: `floor` to round the intermediate calculation down, `mod` to calculate remainder after the division and `reshape` to form the output interleaved data block. The output of the function `interleaver` is interleaved data block after the second permutation. The function `interleaver` is applied to the coded SIGNAL field and coded data part separately.

3.2.5 Subcarrier mapping

The next subcarrier mapping is performed by the function `modulator` with the chosen modulation for the data part of the frame and only the BPSK modulation for the SIGNAL field. The function supports four types of modulations: BPSK, QPSK, 16QAM, and 64QAM. For the BPSK and QPSK modulations, the calculation of the symbols is performed using the for cycle. This cycle is performed with the internal

function `complex` which converts the in-phase and quadrature components to a complex number. Each complex number is the symbol of the constellation diagram. Such complex numbers are accumulated on the output of the function `modulator`. For the 16QAM and 64QAM modulations, the combination of `modem.qammod` and `modulate` internal functions are used. The structure of the QAM modulator `h` is created by the first function. The vector of the mapping symbols is defined based on the Gray coding. Moreover, the type of input data to the modulator is set on the binary format. As a result, the modulation of a given type is performed by the function `modulate` using the previously defined structure `h` and binary input data.

3.2.6 STBC encoder

The next STBC encoder block is used only in case of the MIMO transmission mode. STBC encoder block is implemented using Alamouti space-time code. The channel coefficients matrix is defined by the matrix h in equation 3.1. Previously modulated subcarriers (symbols) are divided into two streams where symbols are transmitted in two different time periods. That procedure is implemented by using for cycle.

$$h = \begin{pmatrix} 1 & 1 \\ 1 & 1 \end{pmatrix} \tag{3.1}$$

3.2.7 OFDM mapping

Next, the OFDM mapping, IFFT, and cyclic prefix insertion blocks are necessary for the OFDM symbol forming. All of these blocks are implemented by the function `ofdm_modulator`. The input of the function contains the modulated symbols and length of the cyclic prefix. The cyclic prefix is chosen by a user. After, the prefix length is calculated due to the choice by the user. After the serial to parallel transformation, the data and pilots mapping into the IFFT block are processed according to the IEEE 802.11 specification. The block IFFT contains 64 subcarriers in total. Twelve subcarriers are related to zeros. Four are related to the pilots, and 48 are related to data. The OFDM symbol without the cyclic prefix is generated using the internal operation `ifft`. The OFDM symbol is copied to its begin based on the length of the normal or short cyclic prefix. The output of the function `ofdm_modulator` is generated with a sequence of such formed OFDM symbols. The OFDM mapping is processed for the modulated SIGNAL field and modulated data part separately. In each OFDM symbol, the length of the cyclic prefix is the same. As a result, the output stream of the OFDM symbols is structured in the SIGNAL, DATA order.

3.2.8 RRC filtering

Next, the RRC (Root Raised Cosine) filtering block is applied for creating the discrete OFDM symbols in the form of analog impulses. Such a block is implemented by the function `RRC_filter`. The core of this function is the RRC filter with necessary parameters for the filtering as the oversampling, delay, roll-off factor, resolution, and number of the samples per the symbol. For the in-phase and quadrature components of the input symbols, the oversampling is implemented by the internal function `upsample`. The optimal oversampling value is chosen 10 to produce enough samples from one side and reduce time of calculations in the simulator from another side. The RRC filter coefficients are created by the internal function `rcosdesign` using optimal parameters as the roll-off factor 0.13, the filter resolution `span` = 60 and the number of the samples per the symbol `sps` = 10. Before the filter processing, the oversampled signal is extended by $\frac{span*sps}{2}$ zeros which products the signal delay in total. To process the filtering with the RRC filter coefficients is used the internal function `filter`. After the filtering, the signal delay is compensated by removing $\frac{span*sps}{2}$ samples from the filtered signal begin. All steps for the RRC filtering are processed for the in-phase and quadrature components separately. The output of the function `RRC_filter` contains the filtered in-phase and quadrature parts of the signal.

3.2.9 IQ modulation

The last block of the transmitter is the IQ modulator. Such a block is implemented by the function `IQ_modulator`. This function converts the filtered signal components to the RF frequency carrier f_c. The same oversampling value as mentioned previously in the RRC filtering block and selected RF frequency carrier are used as the input of this function. In the IQ modulator, one symbol frequency is defined by $f_s = \frac{bandwidth}{64}$. The time vector is defined by t based on the symbol frequency and oversampling parameters. After, the in-phase and quadrature carriers are defined $carrier_I = cos(2 * pi * f_c * t)$ and $carrier_Q = sin(2 * pi * f_c * t)$. Next, the filtered signal is multiplied by the calculated carrier. After summing the products for each the in-phase and quadrature components, the resulted signal is prepared for the transmission by the RF channel.

3.3 Transmission channel

The model of the RF channel is defined between the transmitter and receiver. This model is implemented by the function `RF_channel` with the input parameters: RF

model choice, transmitted signal, signal to noise ratio and symbol frequency. The function supports the AWGN, Rician, Rayleigh and Pedestrian Indoor models of the channel. The carrier-to-noise ratio is used for the AWGN channel and defined by the user in the application.

The AWGN channel is implemented by the internal function `awgn` with the input parameters CNR and signal power, which are calculated before adding the AWGN noise.

In the case of the selective fading channels are defined the necessary fading channel parameters for each model of the channel. The Rician channel model consists of the first direct path and the remain reflected paths on the interval $i =< 1; 11 >$ according to the RC12 model defined in Tab. 2.8. The first path has defined following fading parameters: attenuation $\rho = 1$, delay $\tau = 0\mu s$ and phase shift $\theta = 0$ rad. The fading parameters for the remain paths are given from the Tab. 2.8. The attenuation in a line of sight based on reflection attenuations is calculated by Rician factor $K = 10$ dB. The Rayleigh channel is defined by fading parameters used in the RA12 model has given from Tab. 2.8 for each propagation path. The Rician factor $K = 0$ dB in the Rayleigh channel model. The Pedestrian Indoor channel is defined by fading parameters used in the PI12 model according to Tab. 2.9. The Rician factor is used the same as in the Rician channel model. Speed of the receiver is defined $v = 3$ km/h. The maximum Doppler frequency shift is calculated according to the equation 3.2. Doppler frequency ratio is defined as $fd * 0.5$ and normalized STD deviation is equal to 8%. The sample rate is chosen $Fs = 868$ MHz.

$$f_d = \frac{v * f_c}{3.6 * 300} \tag{3.2}$$

, where f_c is the carrier frequency.

The first Rician part of the PI channel model is defined with *comm.RicianChannel* component with the following parameters [21]:

- 'SampleRate', Fs
- 'NormalizedPathGains', 0
- 'RandomStream','mt19937ar with seed'
- 'Seed',73
- 'KFactor',K
- 'MaximumDopplerShift',fd
- 'DopplerSpectrum',doppler('Gaussian',STD_norm)
- 'PathGainsOutputPort',true

The remain paths are calculated by *comm.RayleighChannel* component with the following parameters:

- 'SampleRate', Fs
- 'NormalizedPathGains', 0

- 'RandomStream','mt19937ar with seed'
- 'Seed',73
- 'MaximumDopplerShift',fd
- 'DopplerSpectrum',doppler('Gaussian',STD_norm)
- 'PathGainsOutputPort',true

3.4 Receiver

3.4.1 IQ demodulation

The first block of the receiver is the IQ demodulator. This block is implemented by the function `IQ_demodulator`. The recovery of the in-phase and quadrature components of the signal is processed based on the carriers for the in-phase and quadrature components of the signal and received signal. Both carriers and received signals are the output of the function `IQ_demodulator`. This output is used for the next communication blocks.

3.4.2 RRC defiltering

The next block is the RRC filtering. To obtain the primary discrete samples is the main purpose of this block. It is implemented by the function `RRC_filter2` with the input parameters downsampling, delay, roll-off factor and both components of the signal. The downsampling parameter is defined as the upsampling parameter in 3.2 by value 10. The delay, roll-off factor, filter span and the number of the samples per the symbol parameters are defined the same as in 3.2. The coefficients of the RRC filter are calculated on the begin using the internal function `rcosdesign`. The delay of the signal is implemented by adding zeros. The filtering itself is implemented by the internal function `filter` using the normalization of the RRC filter coefficients. Next, the compensation of the signal delay is processed by removing $\frac{sps*span}{2}$ zeros from the begin of the signal. After, the downsampling is implemented by the internal function *downsample*. As a result, the output of the function `RRC_filter2` is the sum of the in-phase and quadrature components of the signal.

3.4.3 OFDM demapping

After receiving the discrete samples, the signal is divided into the SIGNAL and DATA parts. First part of the signal SIGNAL is first OFDM symbol with the length $N_{OFDM} = FFT\_size + N_{GI}$ where $FFT\_size = 64$ and N_{GI} depends on the length of the cyclic prefix. The remaining part of the signal is related to the DATA part. Both parts of the signal are processed by the function `ofdm_demodulator`

separately. In this function is processed the serial to parallel conversion based on the length of the OFDM symbol. After, the cyclic prefix is removed. Next, the OFDM symbols without a cyclic prefix are converted to the frequency domain using the internal function `fft`. In the frequency domain, the same number of zero and pilot subcarriers is removed as previously described in 3.2. The output of function `ofdm_demodulator` contains the result which is created using the parallel to serial conversion. This function is based on removing the cyclic prefix, FFT operation and OFDM demapping.

3.4.4 STBC decoder

The next STBC decoder block is used only in case of the MIMO transmission mode. STBC decoder block is implemented using Alamouti space-time code. The channel coefficients matrix is defined by the same matrix h which is previously described in the equation 3.1. Both of the received streams from two antennas are processed using Alamouti code with using channel matrix approximation and maximum likelihood estimation. Whole such procedure is implemented using for cycle with the length of the stream containing modulated symbols.

3.4.5 Subcarrier demapping

Next, the demapping of each subcarrier is processed for each SIGNAL and DATA parts of the signal. It is implemented by the function `demodulator` with an input parameter the type of demodulation. The types of demodulation are the same as the types of modulations which are previously described in 3.2. In the case of the SIGNAL part of the signal is used the BPSK demodulation. In the case of the DATA part of the signal, the demodulation type is the same as the modulation type used in the transmitter. The demapping process for the BPSK and QPSK demodulation is based on removing the normalization factor K_{MOD}, rounding of the received complex numbers using the internal function `round` and the following conversion to the data bits. The output of the function `demodulator` is formed with such accumulated data bits. In the case of 16QAM and 64QAM demodulation, the internal function *modem.qamdemod* is used. This function allows defining the type of demodulation. The result of the function is saved into the variable `h`. Moreover, the parameter $h.SymbolOrder$ is set on $'user - defined'$. The parameter $h.SymbolMapping$ contains the vector of the position of the symbols in the constellation diagram. The parameter $h.OutputType$ is set on the value $'bit'$ to define the binary output. The demapping process is implemented by the internal function `demodulate` together with defined structure `h`. As a result, the output of the function `demodulator` is the output flow of the data bits.

3.4.6 Data deinterleaving

Next block is related to the deinterleaving process. The deinterleaving is applied for the SIGNAL and DATA parts of the signal separately. This block is implemented by the function `deinterleaver` with an input parameter the type of demodulation. Based on the type of demodulation parameters like the number of the coded bits per the OFDM symbol N_{CBPS} and the number of the coded bits per the carrier N_{BPSC} are defined. Such parameters are necessary to form a block of the deinterleaver on the beginning. Moreover, such parameters are used in the double inversion permutation. As a result, the output of the function `deinterleaver` contains a serial flow of the coded data bits.

3.4.7 Data decoding

After the deinterleaving, the block related to the channel decoding is defined. The channel decoding is implemented by the function `fec_decoder` with the input parameter coding rate. The decoder is used for the SIGNAL and DATA parts of the signal separately. In the case of the SIGNAL part of the signal, the coding rate is defined $R = \frac{1}{2}$. For decoding the DATA part of the signal, the coding rate is controlled by the transmission data rate selected by a user in the simulator. The decoder is based on the Viterbi decoding using the internal function `vitdec`. The primarily structure `trellis` is defined with the same parameters which are previously described for the coder in 3.2. In the decoder, *rate_vector* is defined based on the puncturing in the coder. The parameter *rate_vector* is necessary for inserting zeros into defined positions which are related to the coding rate R. Therefore, the operation mode $'trunc'$ is selected to decode with the best metric. This mode is related to the trace depth parameter $tb = 2$. Such value is selected with respect to the operation mode and number of the input symbols of the convolutional decoder. The input type is selected $'hard'$ with respect to the binary data input. Each of the described parameters is used as the input of the function `vitdec`. As a result, the output of the function `fec_decoder` contains the result of the Viterbi decoding.

3.4.8 Data descrambling

The last block is related to the descrambling process which is applied only for the DATA part of the signal. In this phase, the SIGNAL part of the signal is already processed by the receiver. The data descrambling is implemented by the function *descrambler* with the initialization input parameter s corresponding to the initialization parameter s which is described in 3.2. The descrambling process is similar

to the scrambling algorithm. The output of the function *descrambler* contains the same order of the data bits as on the transmitter.

3.5 GUI description

According to Fig. 3.2 GUI program contains the following active parts:

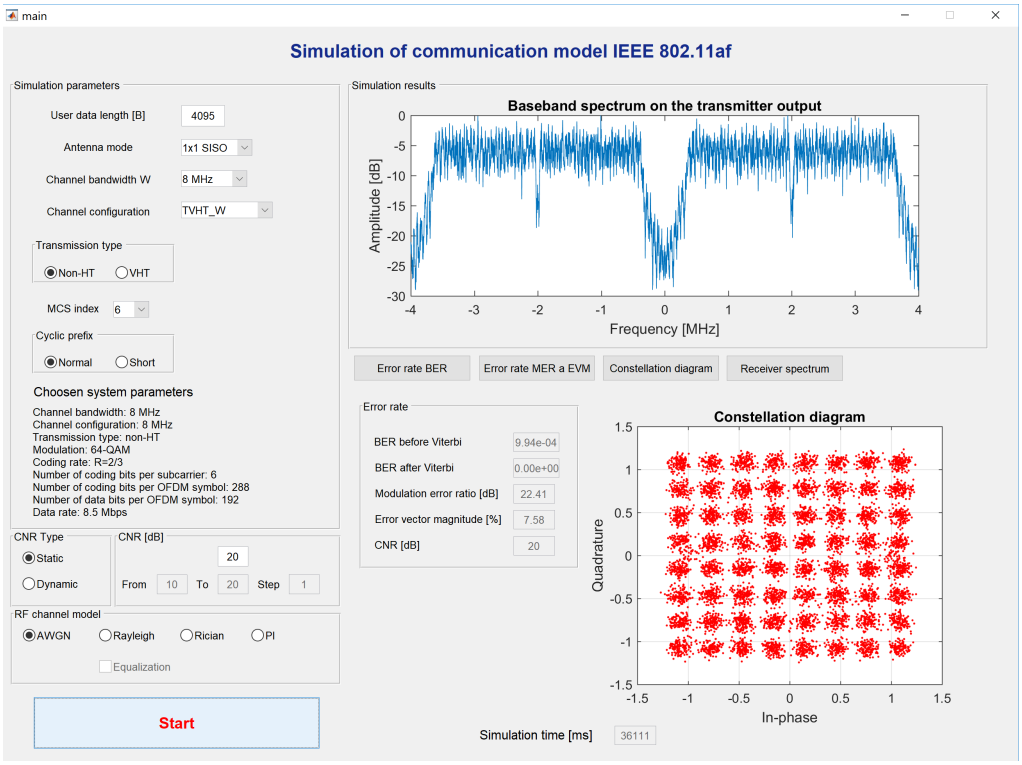

Fig. 3.2: Simulation of the IEEE 802.11af transmitter model.

- Simulation parameters
- CNR type and range of CNR values
- Transmission channel model
- Button Start
- Simulation results

The input simulation parameters contain:

- User data length in bytes
- Antenna mode
- Channel bandwidth
- Channel configuration
- Transmission type
- Transmission rate

- Cyclic prefix

First of all, to start a simulation is necessary to set the input parameters of the model correctly. In the user data length field is inserted the number of data bytes in the range from 0 to 4095 as the input of the communication transmission channel. During simulation, each byte value is generated randomly. In the antenna mode field, two different modes the SISO and MIMO are defined. In the channel bandwidth field, 6, 7 or 8 MHz channels are defined. In the configuration channel field, all possible channel configurations for the IEEE 802.11af standard are defined. The transmission type can be selected as the duplicate non-HT or VHT. In the cyclic prefix field, normal and short prefixes are defined. In the transmission rate field, all possible transmission rates according to the IEEE 802.11af standard are defined. In the field chosen system parameters, the system parameters are printed out such as modulation, coding rate, the number of the coding bits per the subcarrier and number of the coding bits per the OFDM symbol.

Before starting simulation is necessary to select the CNR type which can be static or dynamic. For the static CNR type, one CNR value is enough to define. Otherwise, for the dynamic CNR type have to be defined the range of CNR values. In the transmission channel model field, the following four models are defined: AWGN, Rayleigh, Rician, and PI. For the fading channel models, the channel equalization is also possible to select.

After setting all previously described parameters, the simulation can be started with the button Start. After calculations of the simulation are finished, the frequency spectrum on the transmitter can be found in the simulation results. Moreover, the BER, MER, EVM and constellation diagram on the receiver can be printed out using the corresponding buttons related to the results of the simulation.

For example, following simulation parameters are defined:

- User data length – 4095
- Antenna mode – SISO
- Channel bandwidth – 8 MHz
- Channel configuration – TVHT_W
- Transmission type – Duplicate Non-HT
- Transmission rate – 8.5 Mbps
- Cyclic prefix – Normal

After defining the simulation parameters in the simulator, the chosen system parameters are printed out as the modulation 64QAM, coding rate $R = \frac{2}{3}$, number of the coding bits per the subcarrier 6 and number of the coding bits per the OFDM symbol 288. In the result of simulation according to Fig. 3.2 can be found the frequency spectrum on the transmitter.

4 Simulation results

In this chapter, the results of the simulation in the GUI program are described. In the first part, the basic characteristics of the IEEE 802.11af standard transmission and reception are described considering the AWGN model of the communication channel. To such characteristics belongs to the bit error ratio BER, constellation diagram, and frequency spectrum depending on the carrier-to-noise ratio (CNR). In the next part, the results of the simulation for the fading models of the communication channel are described.

4.1 Test conditions

Before starting the simulation have to be defined the test conditions for the correct simulation. Such conditions ensure the effectiveness of the simulation in terms of time consumption and unambiguity of the simulation. The simulation can be repeated using the conditions described in this chapter. For each simulation, the user data length is defined 4095 B according to the maximum allowed PDDU length in the duplicate non-HT transmission mode. Such selection of the length allows having enough number of symbols in the constellation diagram when 64QAM modulation is used. Moreover, the BER calculations are more precise when a larger amount of data error and transmitted bits are used. The cyclic prefix is set on the normal to achieve maximum elimination of the inter-symbol interference for the IEEE 802.11af standard.

For all simulations except the last one antenna configuration mode is set to the SISO. For the last one simulation, a MIMO 2x2 antenna configuration mode is used. In the BER and MER simulations, BPSK, QPSK, 16QAM, 64QAM and 256QAM modulations for the VHT mode and all of them except the 256QAM modulation for the duplicate non-HT transmission mode are used. To gain such modulations for the duplicate non-HT mode user have to set MCS index to 0, 3, 5 and 7 in the same order and for the VHT mode user have to set MCS indexes to 0, 2, 4, 6 and 8 in the same order. For all the used modulations in the simulation, the coding rate $R = 3/4$ is used except BPSK modulation where is used the coding rate $R = 1/2$. All sets of combinations of modulations, coding rates are based on table 2.1 for duplicate non-HT mode and Appendix A.2 for VHT mode. In most of the simulations, dynamic CNR with the range from 0 to 35 dB with step 1 dB is used. This range is chosen mainly due to having enough content for all used modulations in the simulations. Next important criterion is the time consumption of calculations. In that case, time consumption is calculated in units of minutes.

Simulation of the BER curve is produced in two steps. In the first step, the BER curve is simulated before the Viterbi decoding. In the second step, the BER curve is simulated after the Viterbi decoding. In BER simulations, the BER value is choosen 10^{-4} as reference value. This reference value is choosen the same as for the IEEE 802.11ah standard in diploma thesis [19].

4.2 Simulation in AWGN channel

In this part, the results of the BER, MER curves depending on each type of modulation used in the simulation are described for the model of the AWGN channel. For each simulation, the dynamic CNR type is used in the range of values between 0 and 35 dB with step 1 dB.

4.2.1 BER

The relations between the BER and CNR are presented in duplicate non-HT transmission mode with the BPSK, QPSK, 16QAM, and 64QAM modulations before the Viterbi decoding in Fig. 4.1. BER before the Viterbi decoding is less than 10^{-4} for the BPSK modulation at CNR=6dB, for the QPSK modulation at CNR=10dB, for the 16QAM modulation at CNR=17dB, and for the 64QAM modulation at CNR=22dB.

The relations between the BER and CNR are presented in the VHT transmission mode with the BPSK, QPSK, 16QAM, 64QAM, and 256QAM modulations before the Viterbi decoding in Fig. 4.2. BER before the Viterbi decoding is less than 10^{-4} for the BPSK modulation at CNR=9dB, for the QPSK modulation at CNR=12dB, for the 16QAM modulation at CNR=19dB, for the 64QAM modulation at CNR=25dB and for the 256QAM modulation at CNR=30dB.

Based on these simulations the conclusion is that whole BER before the Viterbi decoding achieves its minimum faster in the case of the BPSK modulation used. Although, the theoretical user data rate for duplicate non-HT mode with MCS index 0 is equals 1.1 Mbps and for VHT mode with MCS index 0 is equals 2.4 Mbps. In the case of the highest order modulation used, the theoretical user data rate for duplicate non-HT mode with MCS index 7 is equals 9.6 Mbps and for VHT mode with MCS index 8 is equals 28.8 Mbps. Besides, the BER in the last case is the highest for small values of the CNR. For correct reception have to be used relatively high values of the CNR.

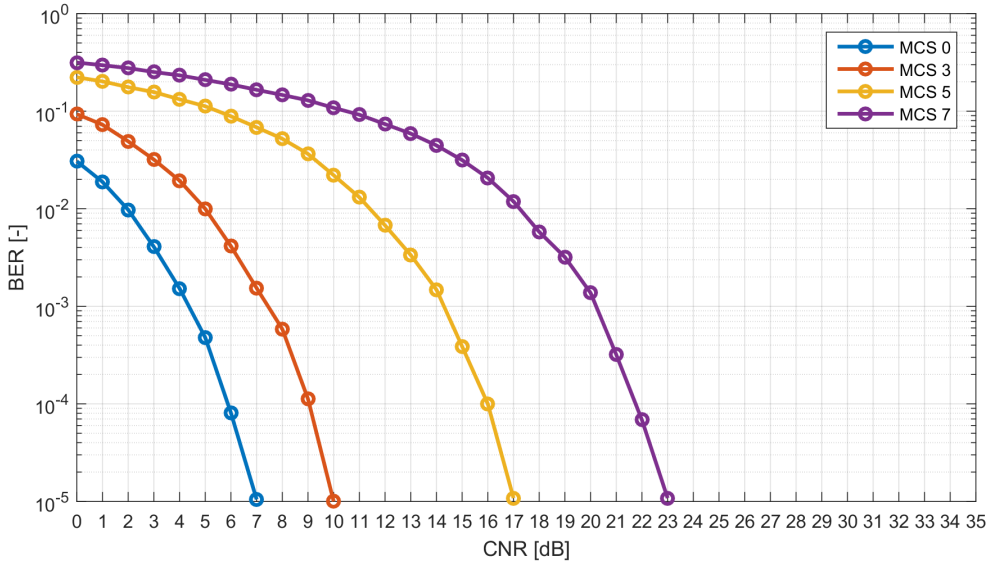

Fig. 4.1: BER before Viterbi decoding for the BPSK, QPSK, 16QAM and 64QAM modulations in the duplicate non-HT mode in the AWGN channel.

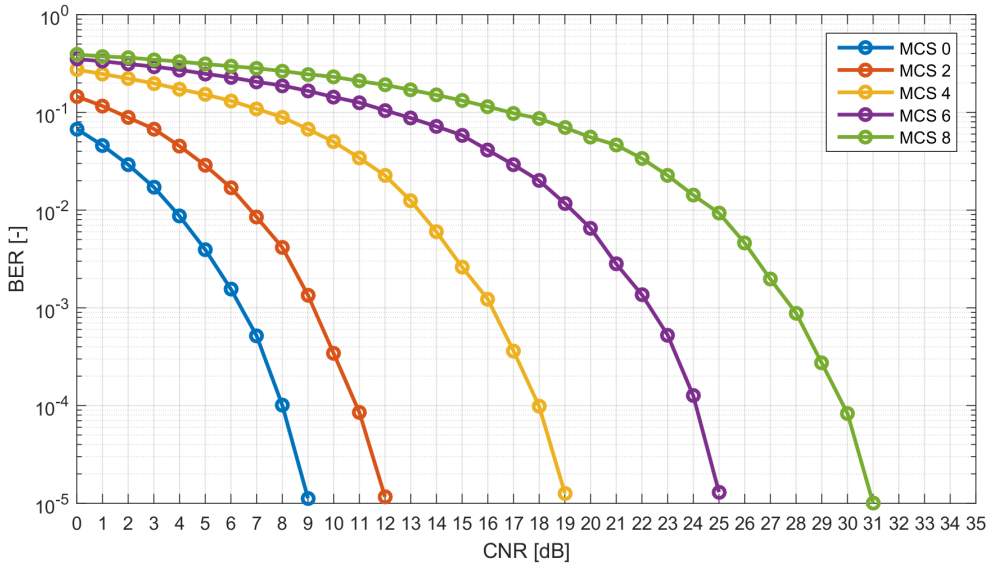

Fig. 4.2: BER before Viterbi decoding for the BPSK, QPSK, 16QAM, 64QAM and 256QAM modulations in the VHT mode in the AWGN channel.

The relations between the BER and CNR are presented for the BPSK, QPSK, 16QAM, and 64QAM modulations after Viterbi decoding in the duplicate non-HT transmission mode in Fig. 4.3. BER after the Viterbi decoding is less than 10^{-4} for the BPSK modulation at CNR=2dB, for the QPSK modulation at CNR=8dB,

for the 16QAM modulation at CNR=14dB, and for the 64QAM modulation at CNR=20dB.

The relations between the BER and CNR are presented for the BPSK, QPSK, 16QAM, 64QAM, and 256QAM modulations after Viterbi decoding in the VHT transmission mode in Fig. 4.4. BER after the Viterbi decoding is less than 10^{-4} for the BPSK modulation at CNR=3dB, for the QPSK modulation at CNR=9dB, for the 16QAM modulation at CNR=15dB, for the 64QAM modulation at CNR=21dB and for the 256QAM modulation at CNR=27dB.

Based on these simulations the conclusion is that whole BER after Viterbi decoding achieves its minimum faster than in the previously described BER before Viterbi decoding. The Viterbi decoding reduces BER on an average by 4 dB for all types of modulation used. In the case of BPSK modulation, the BER is reduced by 6 dB for non-HT duplicate and VHT modes. The main reason is using coding rate $R = \frac{1}{2}$ in comparison with the rest curves where coding rate $R = \frac{3}{4}$ is used.

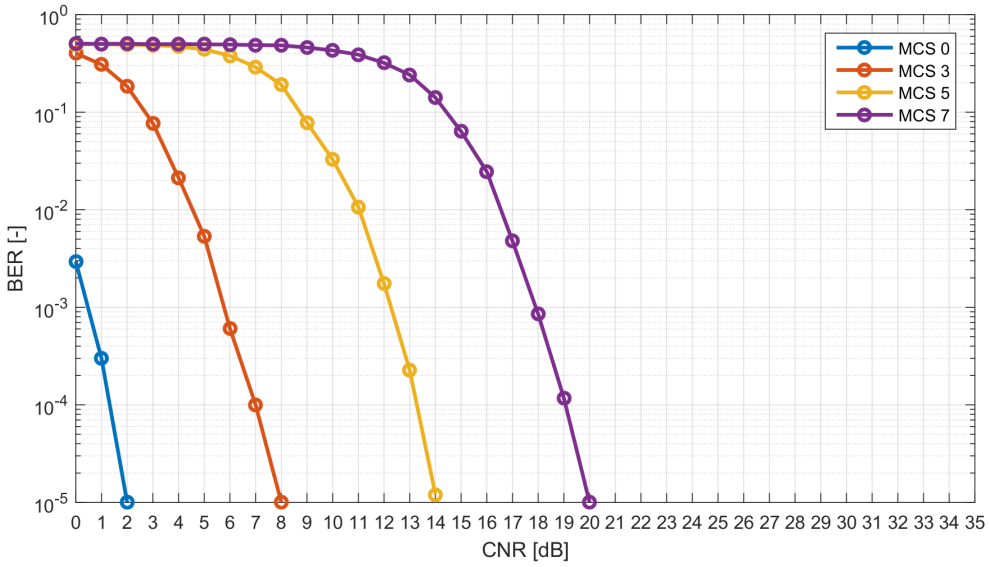

Fig. 4.3: BER after Viterbi decoding for the BPSK, QPSK, 16QAM and 64QAM modulations in the duplicate non-HT mode in the AWGN channel.

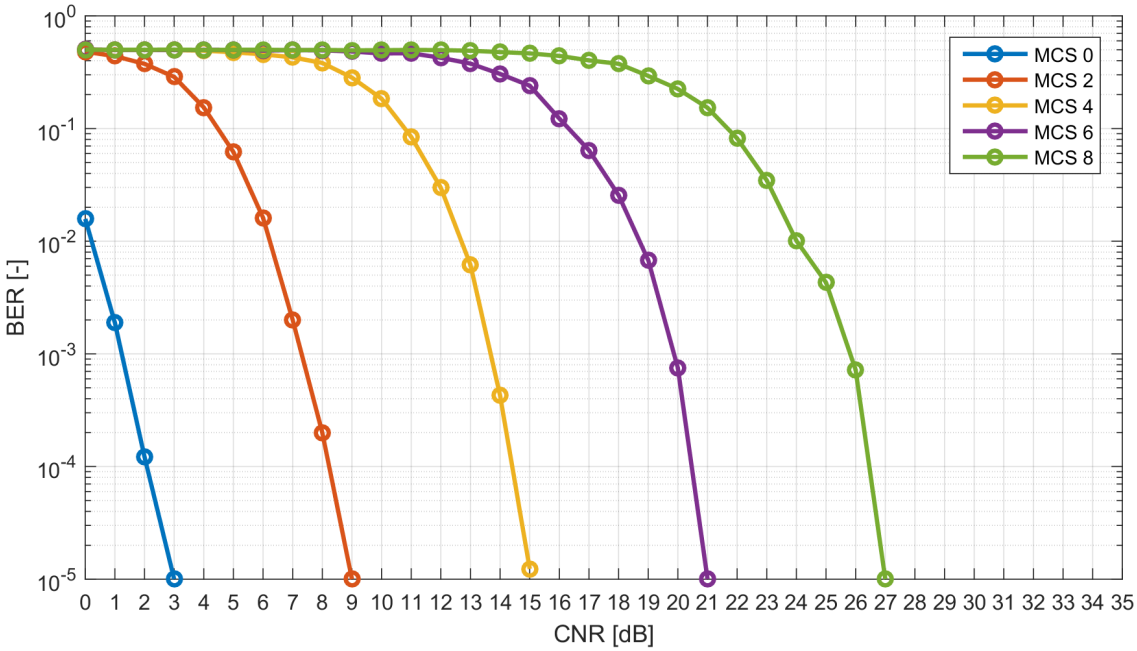

Fig. 4.4: BER after Viterbi decoding for the BPSK, QPSK, 16QAM, 64QAM and 256QAM modulations in the VHT mode in the AWGN channel.

4.2.2 MER

The relations between the MER and CNR are presented for the BPSK, QPSK, 16QAM, and 64QAM modulations in the duplicate non-HT mode in Fig. 4.5. MER value is equal to 12dB at CNR=10dB. As a result, MER value grows linearly with increasing CNR value for each MCS index and different type of modulation.

The relations between the MER and CNR are presented for the BPSK, QPSK, 16QAM, 64QAM, and 256QAM modulations in the VHT mode in Fig. 4.6. MER value is equal to 10dB at CNR=10dB. As a result, MER value grows linearly with increasing CNR value for each MCS index and different type of modulation.

Based on these simulations the conclusion is that MER curves for each type of modulation are the similar to each other. As a result, MER value approximately responses to the CNR value.

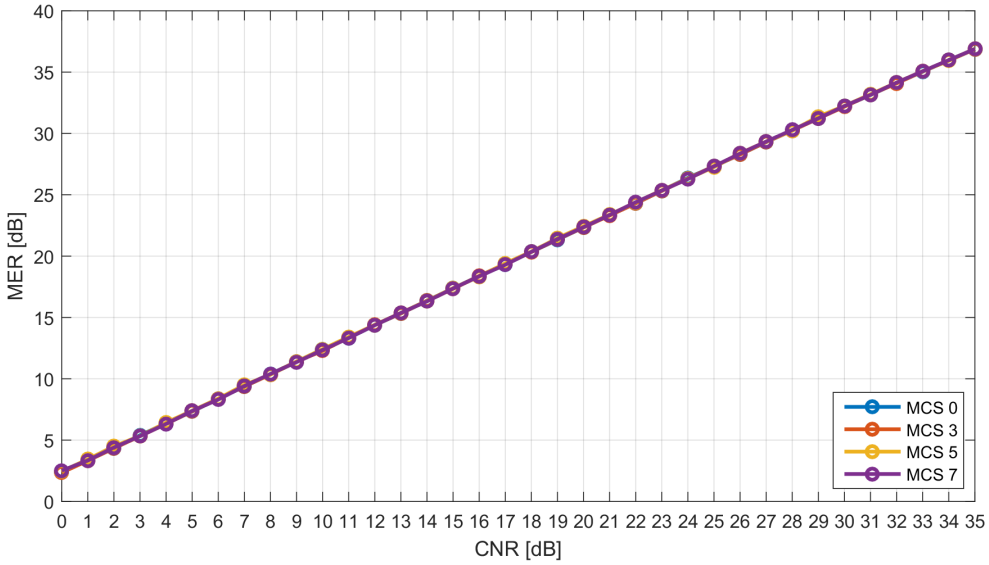

Fig. 4.5: MER for the BPSK, QPSK, 16QAM and 64QAM modulations in the duplicate non-HT mode in the AWGN channel.

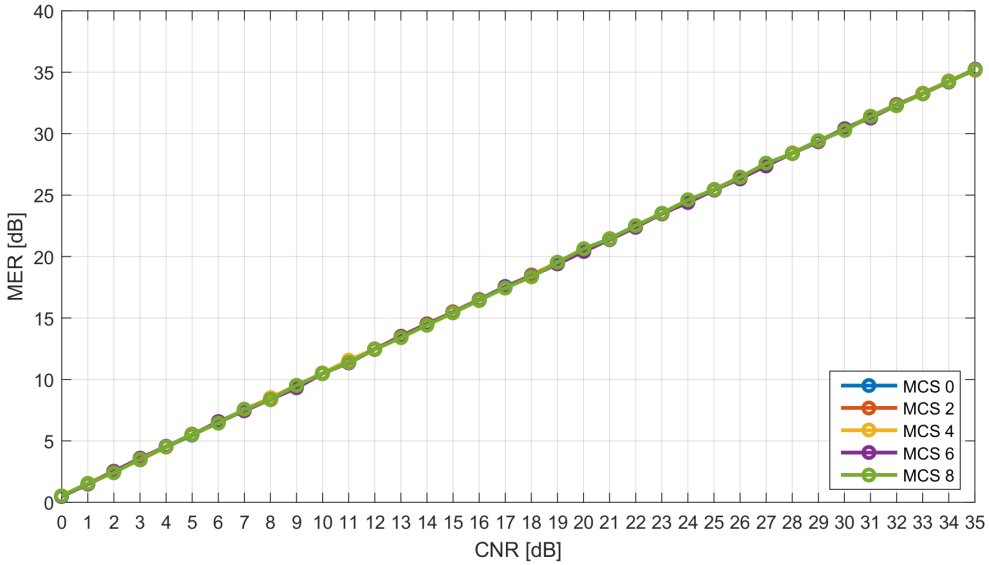

Fig. 4.6: MER for the BPSK, QPSK, 16QAM, 64QAM and 256QAM modulations in the VHT mode in the AWGN channel.

4.2.3 Frequency spectrum

The baseband normalized frequency spectra of the OFDM frames for 6, 7 and 8 MHz of the channel bandwidth are presented in Fig. 4.7. Each spectrum is simulated in the duplicate non-HT mode in the AWGN channel for MCS index 3 with CNR

= 20 dB. As a result, the frequency spectra corresponds with the OFDM mapping described in 2.7.3.

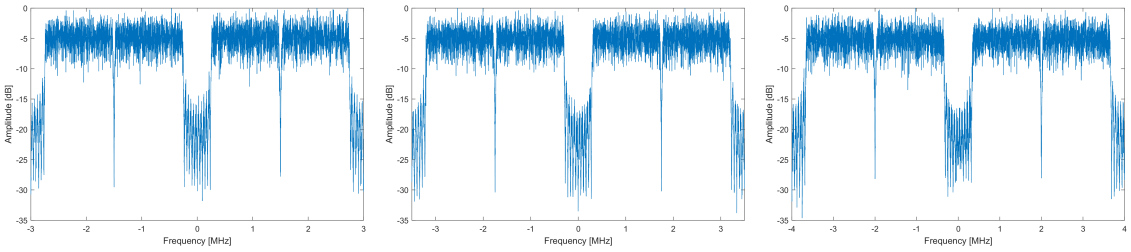

(a) 6 MHz (b) 7 MHz (c) 8 MHz

Fig. 4.7: Baseband frequency spectrum in the duplicate non-HT mode in the AWGN channel

4.2.4 Constellation diagram

The normalized constellation diagrams of the QPSK, 16QAM and 64QAM modulations for 8 MHz of the channel bandwidth are presented in Fig. 4.8. Each constellation diagram is simulated in the duplicate non-HT mode in the AWGN channel with CNR = 25 dB. As a result, the noise is growing with the order of the modulation. Value of MER equals 27 dB for QPSK, 16QAM and 64QAM modulations.

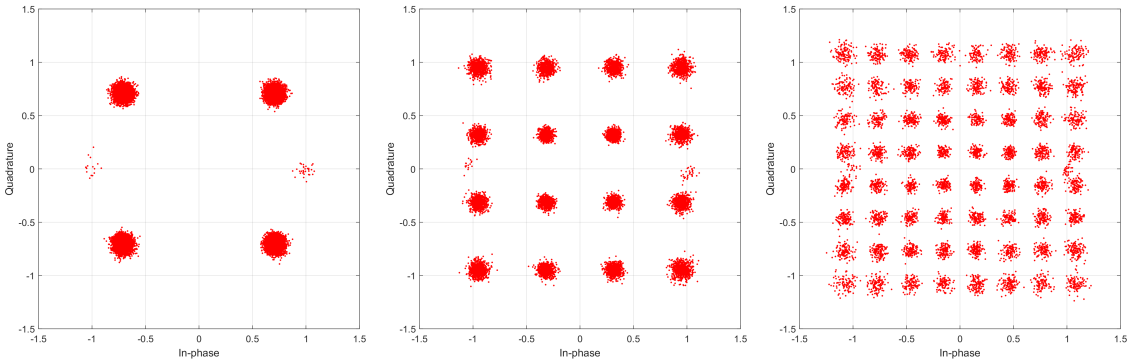

(a) QPSK (b) 16QAM (c) 64QAM

Fig. 4.8: Constellation diagrams in the duplicate non-HT mode in the AWGN channel

4.3 Simulation in Rician channel

In this part, the results of the BER, MER curves depending on each type of modulation used in the simulation are described for the model of the Rician channel. The

BER and MER curves are presented with applying Zero-Forcing equalizer. For each simulation, the dynamic CNR type is used in the range of values between 0 and 35 dB with step 1 dB.

4.3.1 BER

For the duplicate non-HT transmission mode, the calculation of the BER curve is done for MCS indexes 0, 3, 5, and 7 where are used the BPSK, QPSK, 16QAM, and 64QAM modulations.

The relations between the BER and the CNR in the duplicate non-HT transmission mode with the BPSK, QPSK, 16QAM, and 64QAM modulations before the Viterbi decoding are presented in Fig. 4.9. BER before the Viterbi decoding is less than 10^{-4} for the BPSK modulation at CNR=8dB, for the QPSK modulation at CNR=12dB, for the 16QAM modulation at CNR=19dB, and for the 64QAM modulation at CNR=25dB.

The relations between the BER and the CNR in the VHT transmission mode with the BPSK, QPSK, 16QAM, 64QAM, and 256QAM modulations before the Viterbi decoding are presented in Fig. 4.10. BER before the Viterbi decoding is less than 10^{-4} for the BPSK modulation at CNR=9dB, for the QPSK modulation at CNR=13dB, for the 16QAM modulation at CNR=20dB, for the 64QAM modulation at CNR=27dB and for the 256QAM modulation at CNR=33dB.

In comparison with the simulation in the AWGN channel BER before the Viterbi decoding in Rician channel has difference approximately 2 dB for all curves.

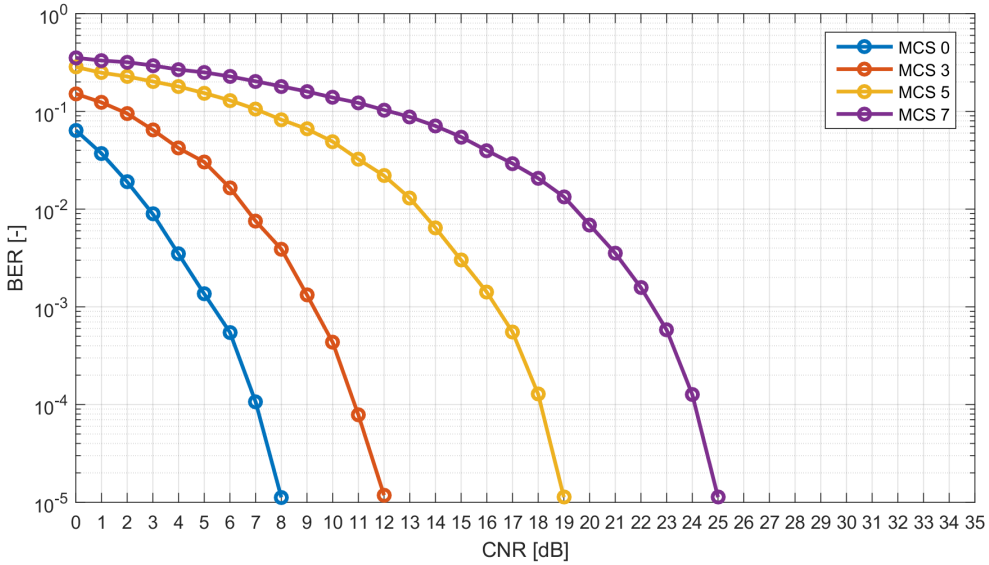

Fig. 4.9: BER before Viterbi decoding for the BPSK, QPSK, 16QAM and 64QAM modulations in the duplicate non-HT mode in the Rician channel.

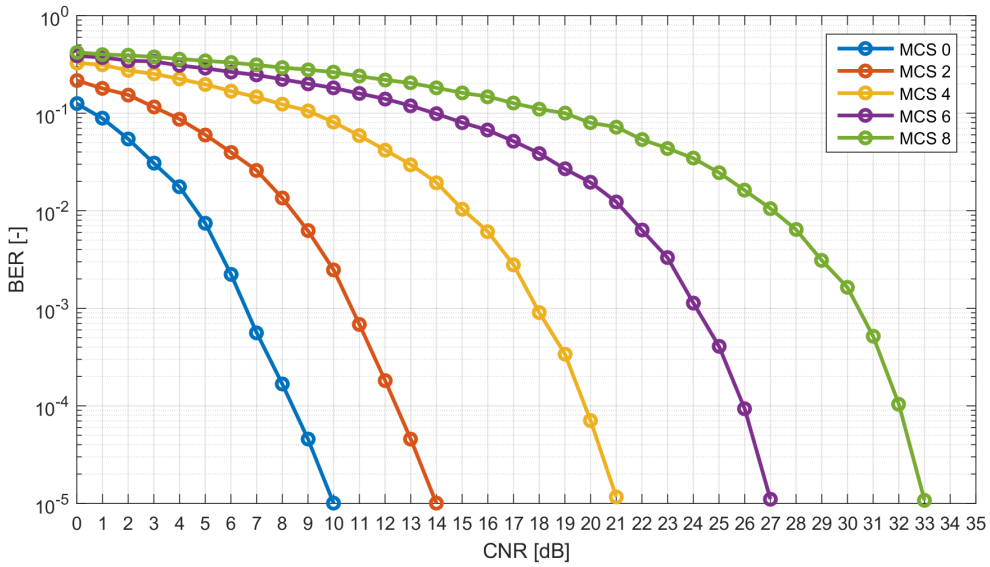

Fig. 4.10: BER before Viterbi decoding for the BPSK, QPSK, 16QAM, 64QAM and 256QAM modulations in the VHT mode in the Rician channel.

The relations between the BER and CNR for the BPSK, QPSK, 16QAM and 64QAM modulations after Viterbi decoding in the duplicate non-HT transmission mode are presented in Fig. 4.11. BER after the Viterbi decoding is less than 10^{-4} for the BPSK modulation at CNR=4dB, for the QPSK modulation at CNR=10dB, for the 16QAM modulation at CNR=16dB, and for the 64QAM modulation at CNR=22dB.

The relations between the BER and CNR for the BPSK, QPSK, 16QAM, 64QAM and 256QAM modulations after Viterbi decoding in the VHT transmission mode are presented in Fig. 4.12. BER after the Viterbi decoding is less than 10^{-4} for the BPSK modulation at CNR=5dB, for the QPSK modulation at CNR=11dB, for the 16QAM modulation at CNR=17dB, for the 64QAM modulation at CNR=23dB and for the 256QAM modulation at CNR=29dB.

The Viterbi decoding reduces BER on an average by 3 dB for all types of modulation used. In the case of the BPSK modulation, the BER is reduced by 5 dB due to robust coding rate used.

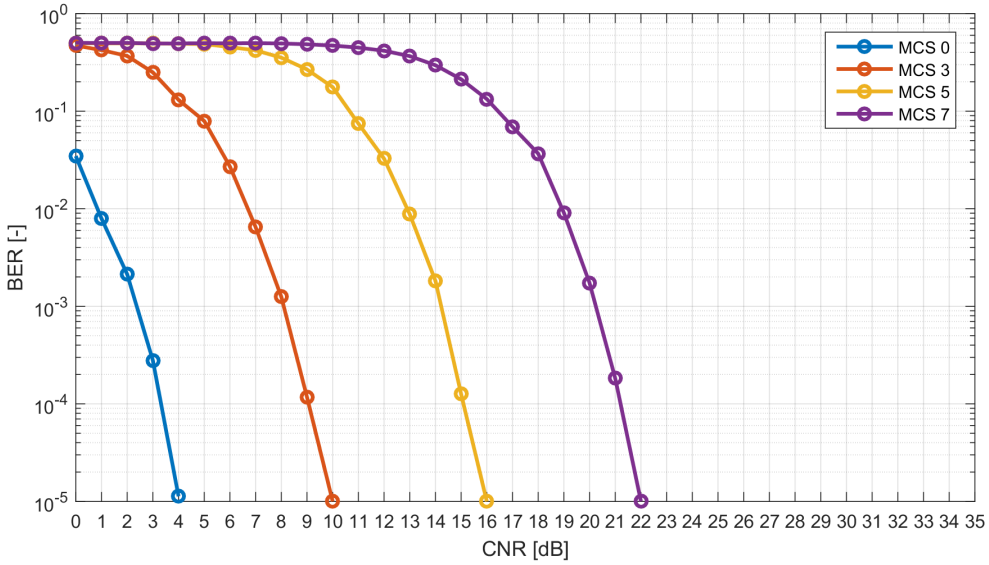

Fig. 4.11: BER after Viterbi decoding for the BPSK, QPSK, 16QAM and 64QAM modulations in the duplicate non-HT mode in the Rician channel.

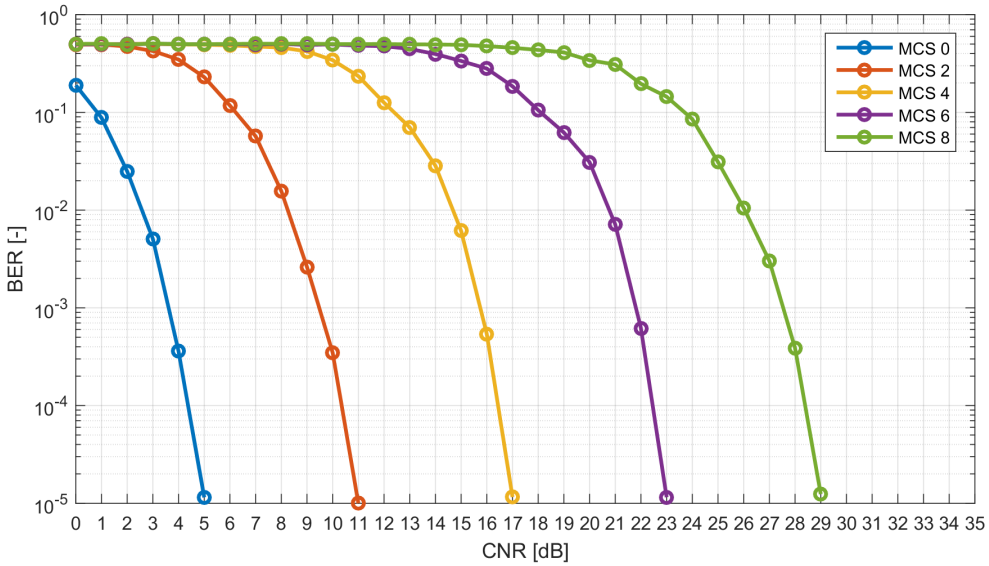

Fig. 4.12: BER after Viterbi decoding for the BPSK, QPSK, 16QAM, 64QAM and 256QAM modulations in the VHT mode in the Rician channel.

4.3.2 MER

The simulations of MER are presented for CNR higher than 5 dB.

The relations between the MER and CNR are presented for the BPSK, QPSK, 16QAM, and 64QAM modulations in the duplicate non-HT mode in Fig. 4.13. MER value is equal to 10dB at CNR=10dB.

The relations between the MER and CNR are presented for the BPSK, QPSK, 16QAM, 64QAM, and 256QAM modulations in the VHT mode in Fig. 4.14. MER value is equal to 8dB at CNR=10dB.

As a result, MER value grows linearly with increasing CNR value for each MCS index and different type of modulation in both transmission modes. Based on these simulations the conclusion is that MER curves for each type of modulation are the similar to each other. As a result, MER value approximately responses to the CNR value.

In comparison with MER curve in AWGN channel MER curve in Rician channel has difference 2 dB for each transmission mode.

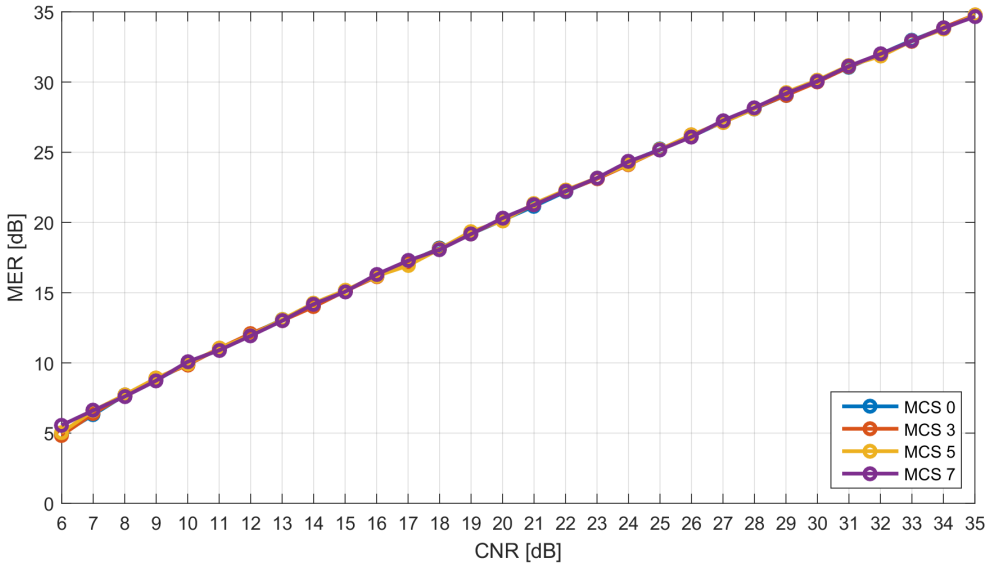

Fig. 4.13: MER for the BPSK, QPSK, 16QAM and 64QAM modulations in the duplicate non-HT mode in the Rician channel.

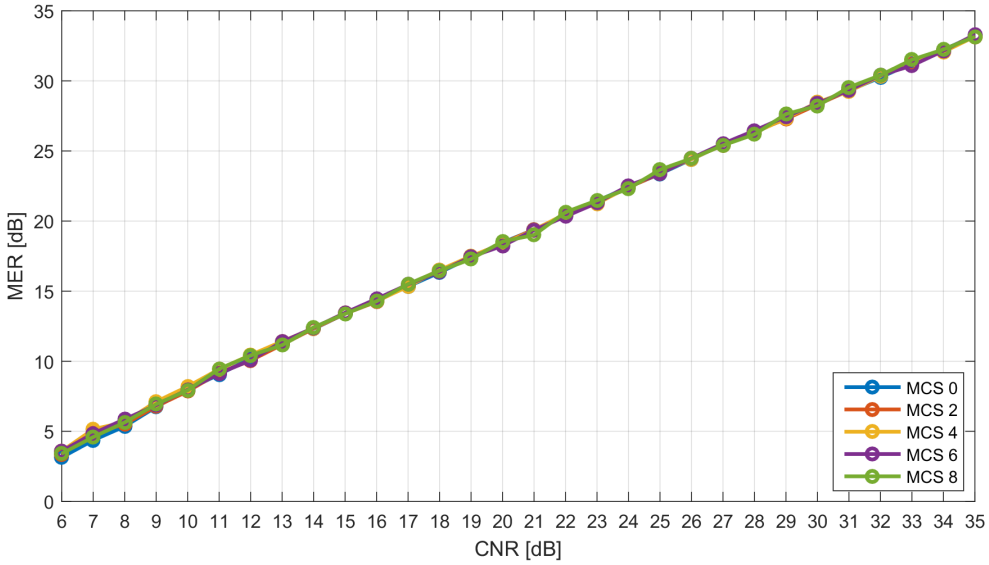

Fig. 4.14: MER for the BPSK, QQPSK, 16QAM, 64QAM and 256QAM modulations in the VHT mode in the Rician channel.

4.3.3 Frequency spectrum

The baseband normalized frequency spectra of the OFDM frames for 6, 7 and 8 MHz of the channel bandwidth are presented in Fig. 4.15. Each spectrum is simulated in Rician channel for MCS index 3 with CNR = 20 dB.

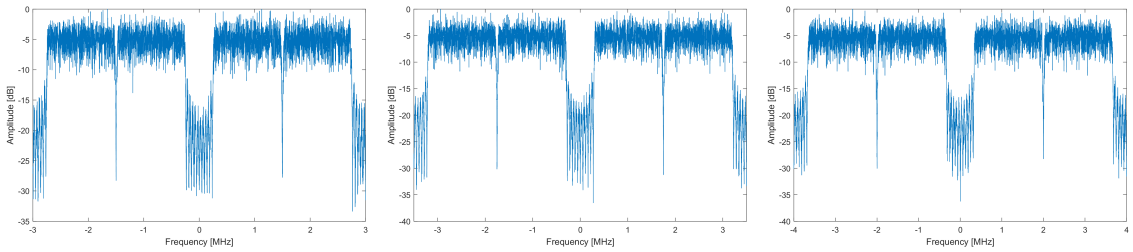

(a) 6 MHz (b) 7 MHz (c) 8 MHz

Fig. 4.15: Baseband frequency spectrum in the duplicate non-HT mode in the Rician channel

4.3.4 Constellation diagram

The normalized constellation diagrams of the QPSK, 16QAM and 64QAM modulations for 8 MHz of the channel bandwidth are presented in Fig. 4.16. Each constellation diagram is simulated in the duplicate non-HT mode in the Rician channel with CNR = 25 dB. As a result, the constellation diagrams are slightly turned due

to phase shift of the signals after propagating in the Rician channel. Value of MER equals approximately 17 dB for QPSK, 16QAM and 64QAM modulations. MER value in the Rician channel is 10dB less than in the AWGN chanel.

The normalized constellation diagrams in the duplicate non-HT mode of the QPSK, 16QAM and 64QAM modulations for 8 MHz of the channel bandwidth are presented in Fig. 4.17. Each constellation diagram is simulated with applying ZF equalizer in the Rician channel with CNR = 25 dB. As a result, the phase shift and attenuation of signals in the Rician channel are corrected and the constellation diagrams corresponds to the constellation diagram in the AWGN channel. Besides, the noise is growing also with the order of the modulation. Value of MER equals approximately 26 dB for QPSK, 16QAM and 64QAM modulations. MER value in the Rician channel is 1dB less than in the AWGN chanel when applying ZF equalization.

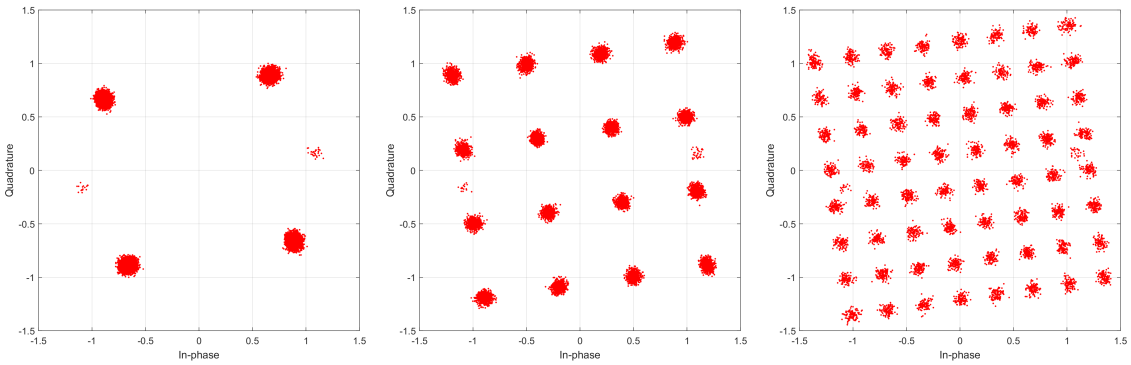

(a) QPSK (b) 16QAM (c) 64QAM

Fig. 4.16: Constellation diagrams in the duplicate non-HT mode in the Rician channel without ZF equalization

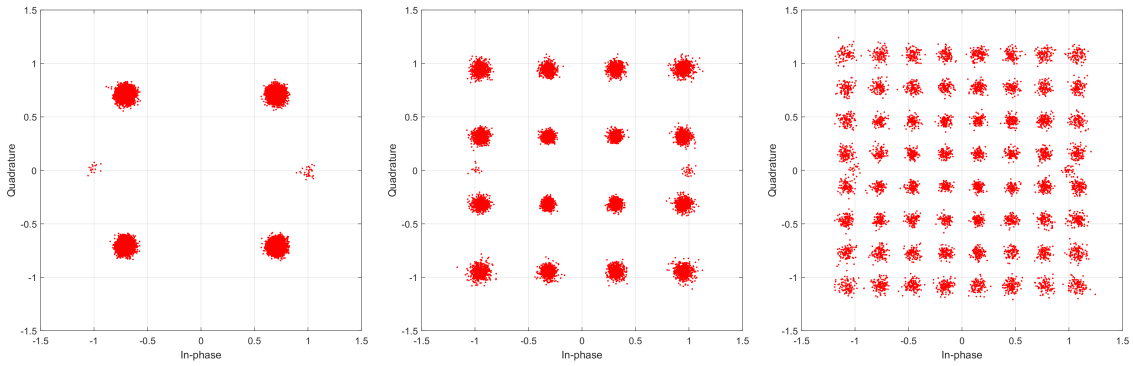

(a) QPSK (b) 16QAM (c) 64QAM

Fig. 4.17: Constellation diagrams in the duplicate non-HT mode in the Rician channel with ZF equalization

4.4 Simulation in Rayleigh channel

In this part, the results of the BER, MER curves depending on each type of modulation used in the simulation are described for the model of the Rayleigh channel. The BER and MER curves are presented with applying Zero-Forcing equalizer. For each simulation, the dynamic CNR type is used in the range of values between 0 and 35 dB with step 1 dB.

4.4.1 BER

The relations between the BER and the CNR in the duplicate non-HT mode with the BPSK, QPSK, 16QAM, and 64QAM modulations before the Viterbi decoding are presented in Fig. 4.18. BER before the Viterbi decoding is less than 10^{-4} for the BPSK modulation at CNR=9dB, for the QPSK modulation at CNR=13dB, for the 16QAM modulation at CNR=20dB, and for the 64QAM modulation at CNR=26dB.

The relations between the BER and the CNR in the VHT mode with the BPSK, QPSK, 16QAM, 64QAM, and 256QAM modulations before the Viterbi decoding are presented in Fig. 4.19. BER before the Viterbi decoding is less than 10^{-4} for the BPSK modulation at CNR=10dB, for the QPSK modulation at CNR=14dB, for the 16QAM modulation at CNR=21dB, for the 64QAM modulation at CNR=27dB and for the 256QAM modulation at CNR=33dB.

In comparison with the simulation in the AWGN channel BER before the Viterbi decoding in Rayleigh channel has difference approximately 3 dB for all curves. In comparison with the simulation in the Rician channel BER before the Viterbi decoding in Rayleigh channel has difference approximately 1 dB for all curves.

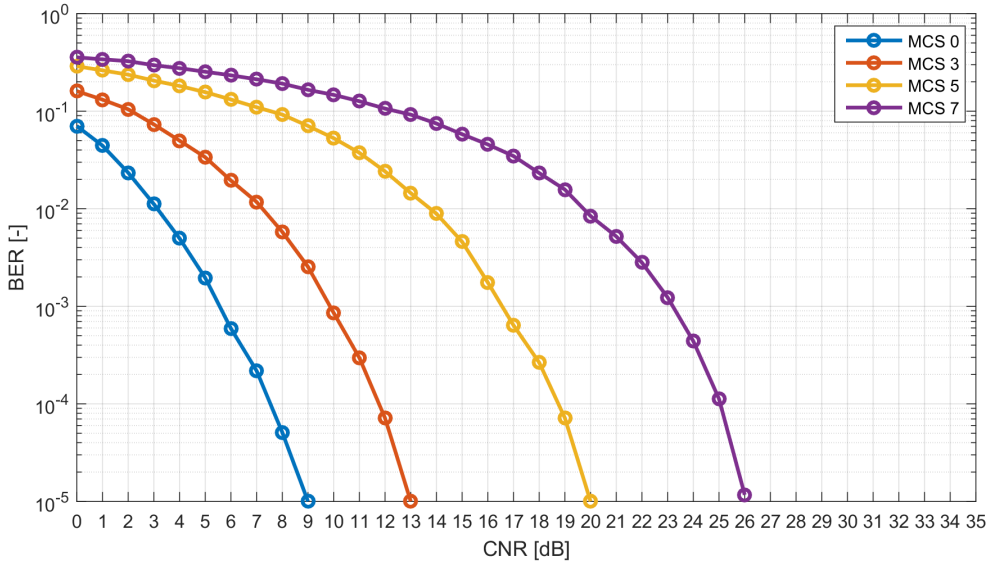

Fig. 4.18: BER before Viterbi decoding for the BPSK, QPSK, 16QAM and 64QAM modulations in the duplicate non-HT mode in the Rayleigh channel.

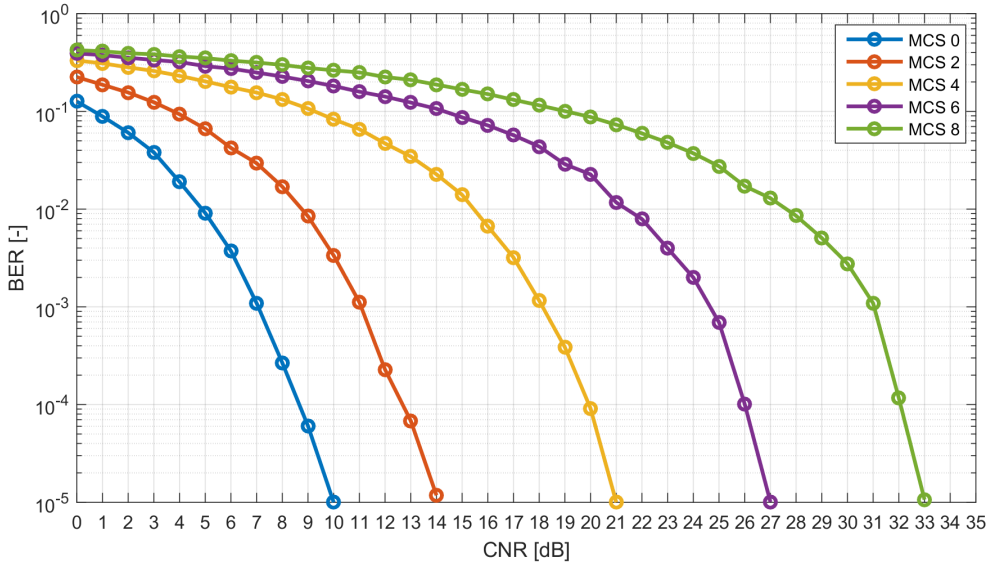

Fig. 4.19: BER before Viterbi decoding for the BPSK, QPSK, 16QAM, 64QAM and 256QAM modulations in the VHT mode in the Rayleigh channel.

The relations between BER and CNR for the BPSK, QPSK, 16QAM and 64QAM modulations after Viterbi decoding in the duplicate non-HT transmission mode are presented in Fig. 4.20. BER after the Viterbi decoding is less than 10^{-4} for the BPSK modulation at CNR=5dB, for the QPSK modulation at CNR=11dB, for the 16QAM modulation at CNR=15dB, and for the 64QAM modulation at CNR=22dB.

The relations between BER and CNR for the BPSK, QPSK, 16QAM, 64QAM and 256QAM modulations after Viterbi decoding in the VHT transmission mode are presented in Fig. 4.21. BER after the Viterbi decoding is less than 10^{-4} for the BPSK modulation at CNR=5dB, for the QPSK modulation at CNR=10dB, for the 16QAM modulation at CNR=17dB, for the 64QAM modulation at CNR=23dB and for the 256QAM modulation at CNR=31dB.

The Viterbi decoding reduces BER on an average by 3 dB for all types of modulation used. In the case of the BPSK modulation, the BER is reduced by 4 dB due to robust coding rate used.

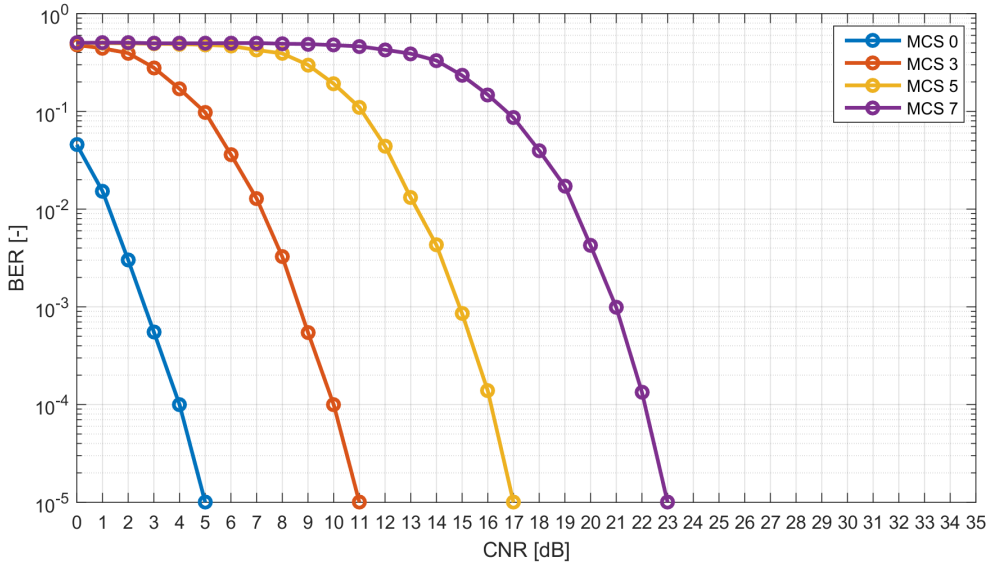

Fig. 4.20: BER after Viterbi decoding for the BPSK, QPSK, 16QAM and 64QAM modulations in the duplicate non-HT mode in the Rayleigh channel.

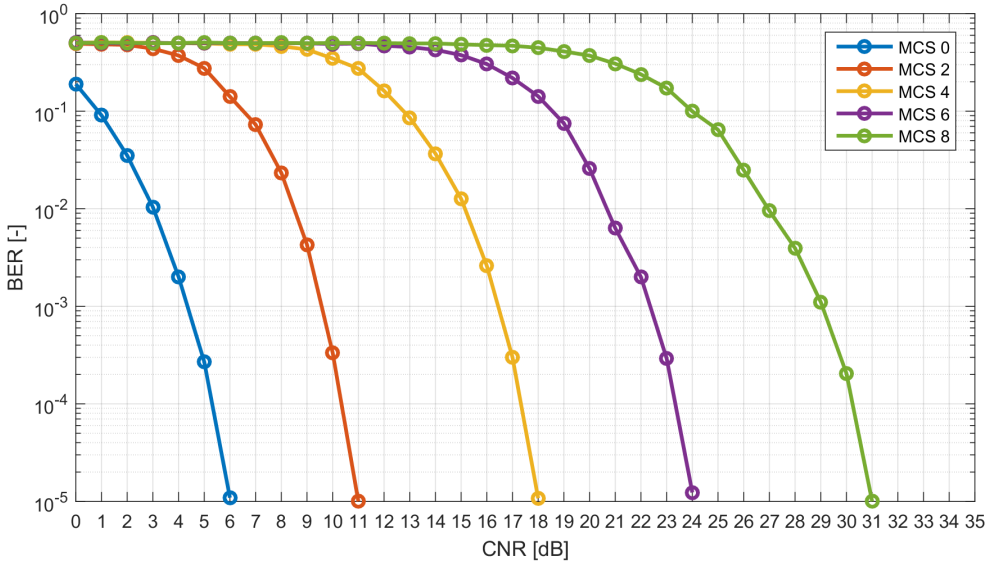

Fig. 4.21: BER after Viterbi decoding for the BPSK, QPSK, 16QAM, 64QAM and 256QAM modulations in the VHT mode in the Rayleigh channel.

4.4.2 MER

The simulations of MER are presented for CNR higher than 5 dB.

The relations between the MER and CNR are presented for the BPSK, QPSK, 16QAM, and 64QAM modulations in the duplicate non-HT mode in Fig. 4.22. MER value is equal to 9dB at CNR=10dB.

The relations between the MER and CNR are presented for the BPSK, QPSK, 16QAM, 64QAM, and 256QAM modulations in the VHT mode in Fig. 4.23. MER value is equal to 7dB at CNR=10dB.

In comparison with MER curve in AWGN channel MER curve in Rician channel has difference approximately 3 dB for each transmission mode. In comparison with MER curve in Rician channel MER curve in Rayleigh channel has difference approximately 1 dB for each transmission mode. It is important to note that the tendency of the MER curve after approximately CNR = 30 dB is not linear for both transmission modes.

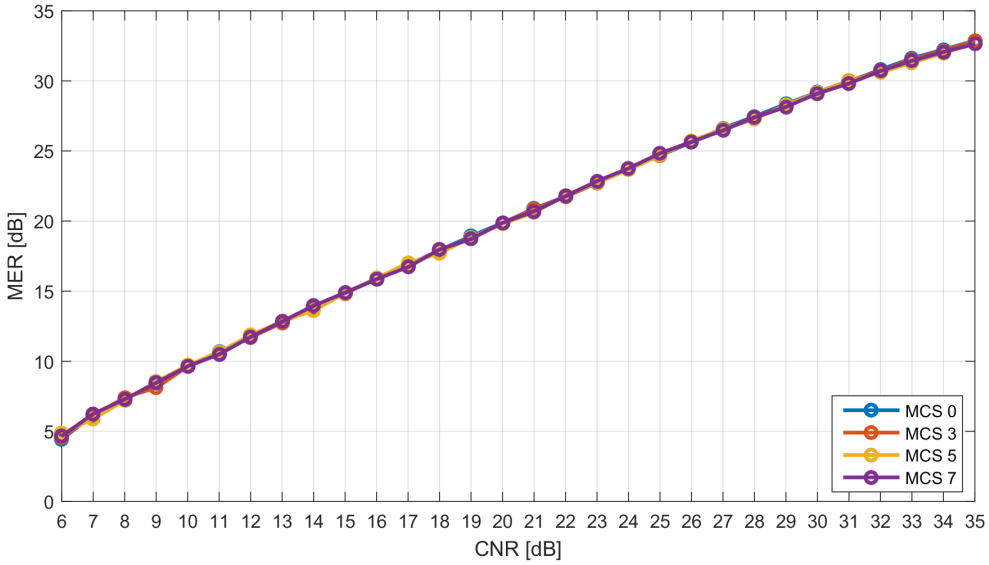

Fig. 4.22: MER for the BPSK, QPSK, 16QAM and 64QAM modulations in the duplicate non-HT mode in the Rayleigh channel.

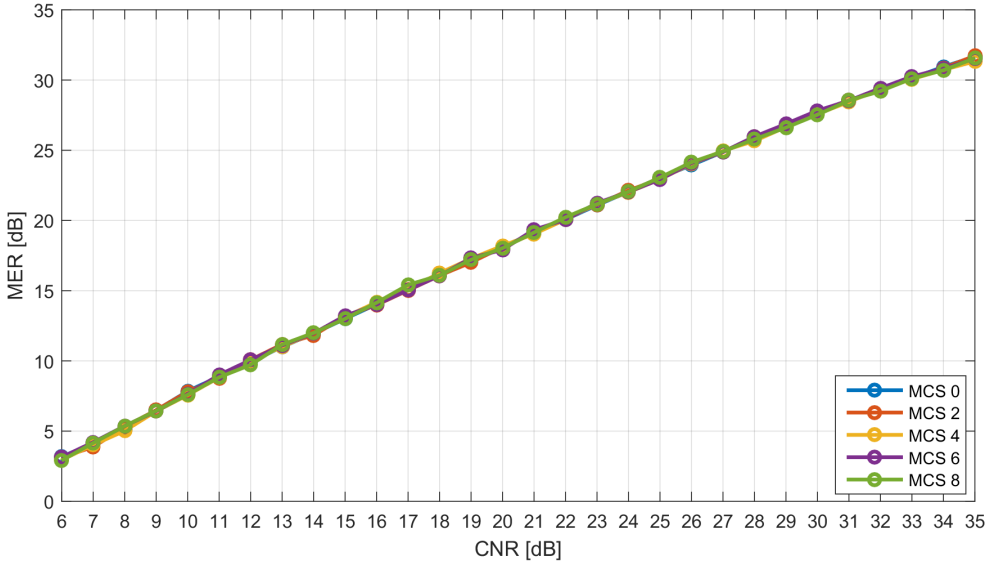

Fig. 4.23: MER for the BPSK, QPSK, 16QAM, 64QAM and 256QAM modulations in the VHT mode in the Rayleigh channel.

4.4.3 Frequency spectrum

The baseband normalized frequency spectra of the OFDM frames for 6, 7 and 8 MHz of the channel bandwidth are presented in Fig. 4.24. Each spectrum is simulated in

the duplicate non-HT mode in Rayleigh channel for MCS index 3 with CNR = 20 dB.

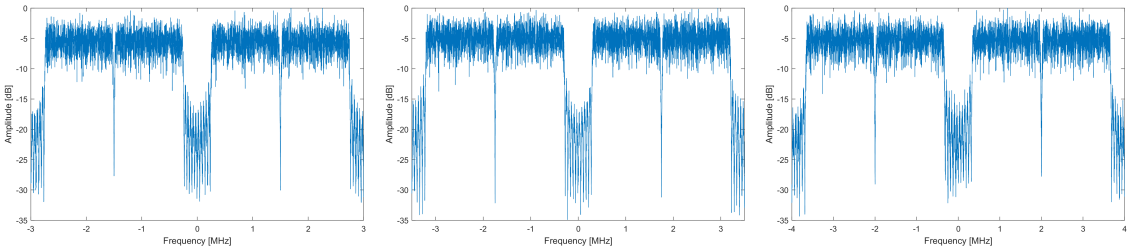

(a) 6 MHz (b) 7 MHz (c) 8 MHz

Fig. 4.24: Baseband frequency spectrum in the duplicate non-HT mode in the Rayleigh channel

4.4.4 Constellation diagram

The normalized constellation diagrams of the QPSK, 16QAM and 64QAM modulations for 8 MHz of the channel bandwidth are presented in Fig. 4.25. Each constellation diagram is simulated in the duplicate non-HT mode in the Rayleigh channel with CNR = 25 dB. As a result, the constellation diagrams are significantly turned due to phase shift of the signals after propagating in the Rayleigh channel. Besides, constellation points are stretched in the constellation diagrams. Value of MER equals approximately -3 dB for QPSK, 16QAM and 64QAM modulations. MER value in the Rayleigh channel is 30 dB less than in the AWGN chanel when applying ZF equalization.

The normalized constellation diagrams in the duplicate non-HT mode of the QPSK, 16QAM and 64QAM modulations for 8 MHz of the channel bandwidth are presented in Fig. 4.26. Each constellation diagram is simulated with applying ZF equalizer in the Rayleigh channel with CNR = 25 dB. As a result, the phase shift and attenuation of signals in the Rayleigh channel are well corrected and the constellation diagrams corresponds to the constellation diagram in the AWGN channel. Value of MER equals approximately 25 dB for QPSK, 16QAM and 64QAM modulations. MER value in the Rayleigh channel is 2 dB less than in the AWGN chanel and 1 dB less than in the Rician channel when applying ZF equalization.

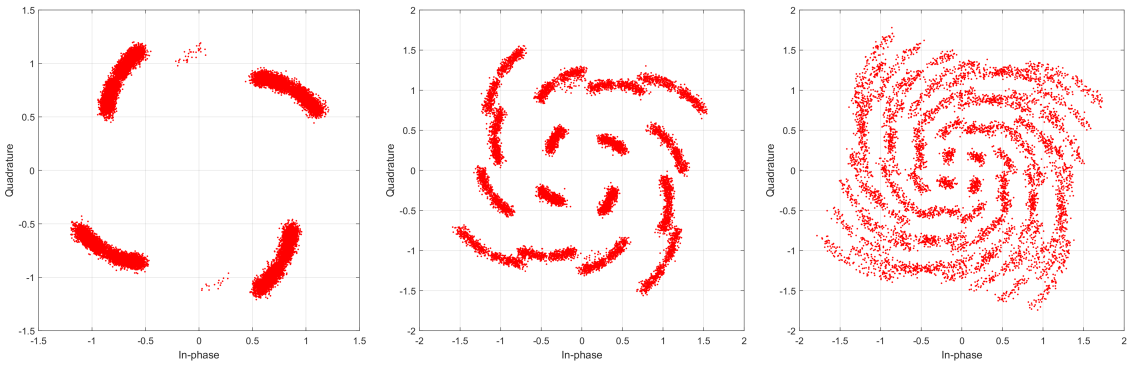

(a) QPSK (b) 16QAM (c) 64QAM

Fig. 4.25: Constellation diagrams in the duplicate non-HT mode in the Rayleigh channel without ZF equalization

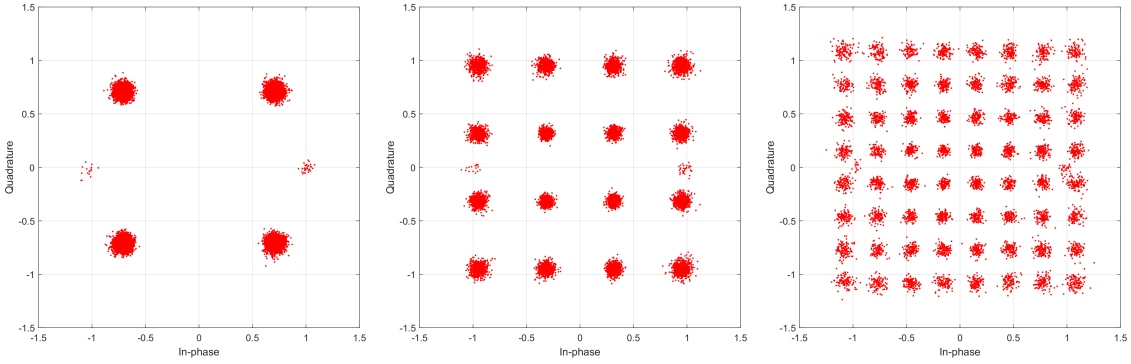

(a) QPSK (b) 16QAM (c) 64QAM

Fig. 4.26: Constellation diagrams in the duplicate non-HT mode in the Rayleigh channel with ZF equalization

4.5 Simulation in MIMO 2x2 mode

In this part, the results of the BER, MER curves depending on each type of modulation used in the simulation are described for the model of the AWGN channel in MIMO 2x2 transmission mode. All the results are provided in the duplicate non-HT mode. For each simulation is used the dynamic CNR type in the range of values between 0 and 14 dB with step 1 dB.

4.5.1 BER

The relations between the BER and CNR before the Viterbi decoding are presented in Fig. 4.27 for the supported by the IEEE 802.11af standard the BPSK, QPSK,

16QAM, and 64QAM modulations. BER before the Viterbi decoding is less than 10^{-4} for the BPSK modulation at CNR=2dB and for the QPSK modulation at CNR=5dB.

In comparison with the BER in the AWGN channel using SISO antenna configuration the BER in the AWGN channel using MIMO 2x2 antenna configuration has difference approximately 4 dB for all modulation used.

The relations between the BER and CNR are presented in Fig. 4.28 for the BPSK, QPSK, 16QAM and 64QAM modulations after Viterbi decoding. BER after the Viterbi decoding is less than 10^{-4} for the BPSK modulation at CNR=0dB and for the QPSK modulation at CNR=3dB.

The Viterbi decoding reduces BER on an average by 4 dB for all types of modulation used. In the case of the BPSK modulation, the BER is reduced by 5 dB due to robust coding rate used. In the case of the BPSK modulation, the BER value is the least of all simulations for the MIMO 2x2 antenna mode and not presented due to that reason.

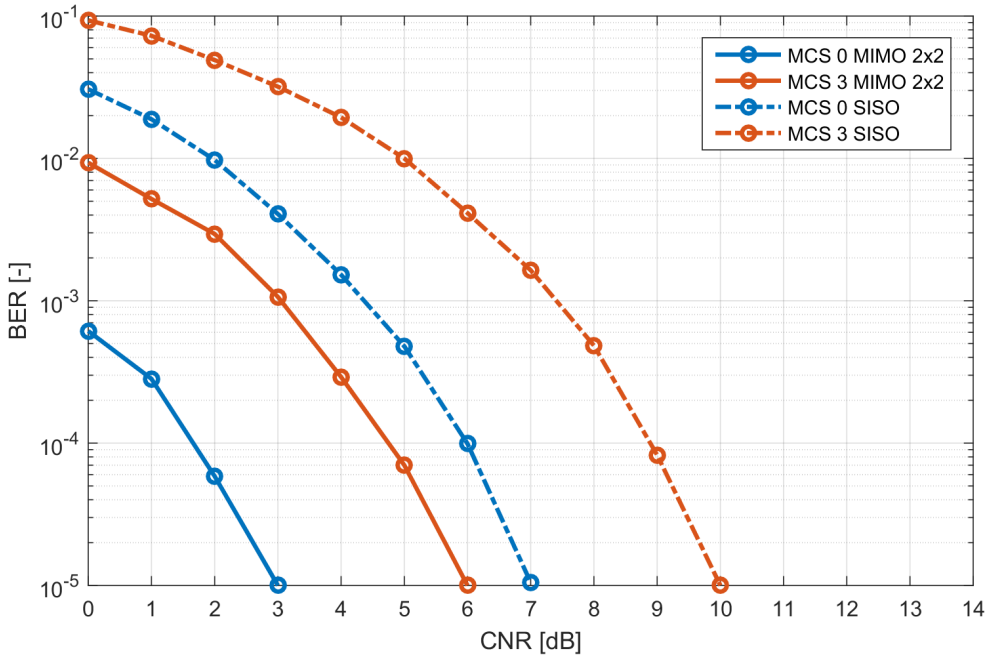

Fig. 4.27: Comparison of BER before Viterbi decoding between MIMO 2x2 and SISO antenna modes for the MCS indexes 0 and 3 in the duplicate non-HT mode in the AWGN channel.

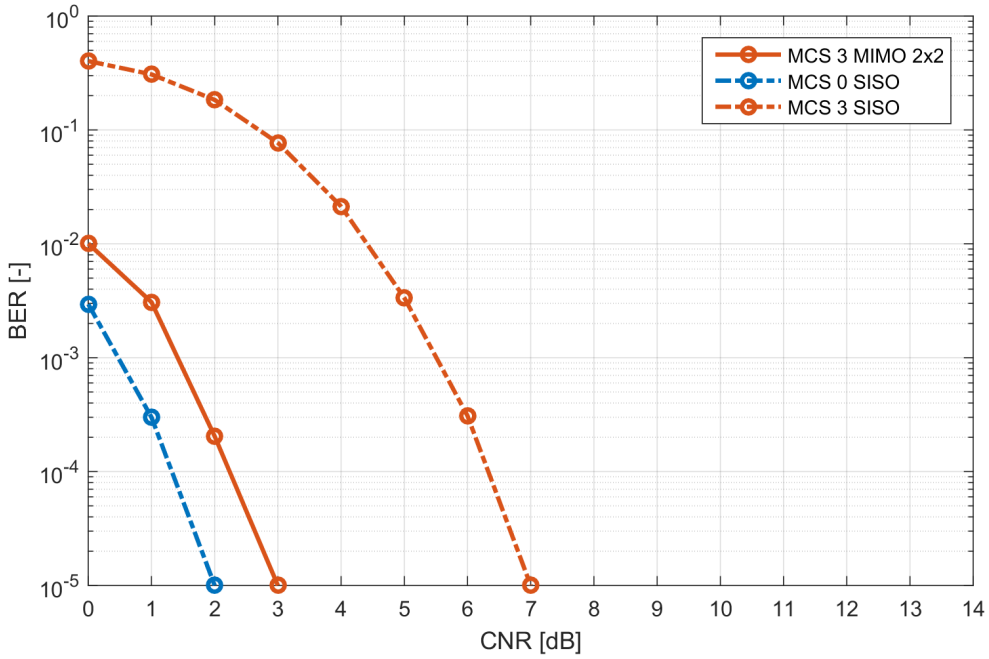

Fig. 4.28: Comparison of BER after Viterbi decoding between MIMO 2x2 and SISO antenna modes for the MCS indexes 0 and 3 in the duplicate non-HT mode in the AWGN channel.

5 Conclusion

In the current diploma thesis is designed simulation model of the wireless communication system defined by the IEEE 802.11af standard. Thank to the analysis of the physical layer of the IEEE 802.11af standard were described the following transmitter components for such a system: data scrambler, convolutional encoder, interleaver, subcarrier mapping, STBC encoder, OFDM mapping, RRC filtering, and IQ modulator. Moreover, for the receiver are considered following equivalent components to the transmitter components in the opposite order: IQ demodulator, RRC defiltering, OFDM demapping including equalization, STBC decoder, subcarrier demapping, inversion interleaving, convolutional decoding, data descrambler. All of these components are necessary for the correct implementation of the transmitter and receiver of the IEEE 802.11af communication model. For the following simulations of the wireless transmission were described AWGN channel and frequency selective channel models such as Rician, Rayleigh and Pedestrian Indoor for simulating fixed and portable receptions. In addition, were described LDPC encoder and CSD components as a possible option in the IEEE 802.11af standard. The description of the current communication model is based on the mandatory duplicate non-HT transmission mode. Moreover, in the thesis is described the second VHT transmission mode for high throughput transmission of the IEEE 802.11af standard.

The previously described components of the communication model are designed and implemented in the form of GUI simulator in the MATLAB programming environment. In the communication model are implemented transmission modes SISO and MIMO 2x2. The system parameters choice of the physical layer is based on the modulation coding schemes defined in the IEEE 802.11af standard. The communication model is implemented according to the designed block diagram in chapter 3. The implementation of each component from that block diagram is described in details also in chapter 3. Moreover, in the same chapter is described handling with the graphical user interface of the simulator. The simulator allows choose previously described models of the wireless communication channel. It gives opportunity to explore results of the simulations for the different channel models. In addition, the simulator also supports different BCU bandwidths (6, 7 and 8 MHz) which could be used for the current regulatory domain. By selecting the wider BCU bandwidth 8 MHz can be achieved the higher user data throughput than in the rest BCU bandwidths.

In chapter 4 are described results of the simulations which were produced by the created GUI simulator. Such results of the simulations are provided using estimation of the IEEE 802.11af communication model by the following simulations: BER before and after Viterbi decoding, MER, frequency spectrum and constellation dia-

gram. The simulation results are provided and analyzed for all previously described models of the communication channel except Pedestrian Indoor model of channel due to absence of relevant information especially for the IEEE 802.11af standard and time reasons on its implementation. Moreover, the results are provided for system configuration MIMO 2x2. As a result, the choosing antenna mode MIMO 2x2 allows improving the user data throughput and the reception quality having less BER than in the SISO mode.

The main advantage of this GUI simulator is variety of possibilities to select system parameters to simulate different scenarios of the IEEE 802.11af communication model. The interface of this simulator has intuitive and simple handling.

This thesis deals with MIMO 2x2 antenna configuration and one channel bandwidth which unfortunately limits the user data throughput. To improve the user data throughput can be considered more complex contiguous and non-contiguous channel configurations which the IEEE 802.11af standard also provides. By the optimizing the GUI program can be achieved faster and effective its work.

Bibliography

[1] FLORES, Adriana B., Ryan E. GUERRA, Edward W. KNIGHTLY, Peter ECCLESINE and Santosh PANDEY. IEEE 802.11af: a standard for TV white space spectrum sharing. *IEEE Communications Magazine* [online]. 2013, vol. 51, no. 10, pp. 92-100 [cit. 2019-05-01]. DOI: 10.1109/MCOM.2013.6619571. ISSN 0163-6804. Available at: <https://ieeexplore.ieee.org/document/6619571>.

[2] MILOS, Jiri, Ladislav POLAK, Martin SLANINA and Tomas KRATOCHVIL. Link-level simulator for WLAN networks. In: *2016 1st International Workshop on Link- and System Level Simulations (IWSLS)* [online]. IEEE, 2016, 2016-7-1, pp. 1-4 [cit. 2019-05-01]. DOI: 10.1109/IWSLS.2016.7801576. ISBN 978-1-5090-4949-3. Available at: <http://ieeexplore.ieee.org/document/7801576/>.

[3] VILLARDI, Gabriel, Chin-Sean SUM, Chen SUN, Yohannes ALEMSEGED, Zhou LAN and Hiroshi HARADA. Efficiency of dynamic frequency selection based coexistence mechanisms for tv white space enabled cognitive wireless access points. *IEEE Wireless Communications* [online]. vol. 19, no. 6, pp. 69-75 [cit. 2019-05-01]. DOI: 10.1109/MWC.2012.6393520. ISSN 1536-1284. Available at: <http://ieeexplore.ieee.org/document/6393520/>.

[4] IEEE 802.11af White-Fi Technology. *Electronics-notes.com* [online]. [cit. 2019-05-01]. Available at: <https://www.electronics-notes.com/articles/connectivity/wifi-ieee-802-11/802-11af-white-fi.php>.

[5] MITOLA, J. and G.Q. MAGUIRE. Cognitive radio: making software radios more personal. *IEEE Personal Communications* [online]. vol. 6, no. 4, pp. 13-18 [cit. 2019-05-01]. DOI: 10.1109/98.788210. ISSN 1070-9916. Available at: <http://ieeexplore.ieee.org/document/788210/>.

[6] LEKOMTCEV, Demian and Roman MARŠÁLEK. Comparison of 802.11af and 802.22 standards – physical layer and cognitive functionality. *Elektrorevue* [online]. 2012, vol. 3, no. 2, pp. 12-18 [cit. 2019-05-01]. ISSN 1213-1539.

[7] *IEEE Standard for Information technology: Part 11: Wireless LAN Medium Access Control (MAC) and Physical Layer (PHY) Specifications*. Revision of IEEE Std 802.11-2012. New York: IEEE Computer Society, 2016.

[8] PHY Basics: How OFDM Subcarriers Work. *Revolutionwifi.net* [online]. [cit. 2019-05-01]. Available at: <http://www.revolutionwifi.net/revolutionwifi/2015/3/how-ofdm-subcarriers-work>.

[9] MIMO Formats - SISO, SIMO, MISO, MU-MIMO. *Electronics-notes.com* [online]. [cit. 2019-05-01]. Available at: <https://www.electronics-notes.com/articles/antennas-propagation/mimo/siso-simo-miso-mimo.php>.

[10] KRATOCHVÍL, Tomáš. *Digitální televizní a rozhlasové systémy*. Brno: Brno university of technology. Faculty of electrical engineering and communication. Department of radio electronics, 2012. 268 pages. ISBN 978-80-214-4501-7.

[11] ZAINUDIN, Ahmad, Amang SUDARSONO a I Gede Puja ASTAWA. Performance Analysis of an OFDM PHY Scheme with Zero Forcing Equalizer Using Software Defined Radio Platform and USRP. *EMITTER International Journal of Engineering Technology* [online]. 2014, vol. 2, no. 1 [cit. 2019-05-01]. DOI: 10.24003/emitter.v2i1.15. ISSN 2443-1168. Available at: <https://emitter.pens.ac.id/index.php/emitter/article/view/15>.

[12] *IEEE Standard for Information technology: Part 11: Wireless LAN Medium Access Control (MAC) and Physical Layer (PHY) Specifications*. Amendment 5: Enhancements for Higher Throughput. New York: IEEE Computer Society, 2009, 560 pages.

[13] HASSAN, Emad S. *Multi-carrier communication systems with examples in MATLAB: a new perspective*. Boca Raton: CRC Press, 2016. ISBN 9781498735322.

[14] SANTUMON, S.D. Space-Time Block Coding (STBC) for Wireless Networks. *International Journal of Distributed and Parallel systems* [online]. 2012, vol. 3, no. 4, pp. 183-195 [cit. 2019-05-01]. DOI: 10.5121/ijdps.2012.3419. ISSN 22293957. Available at: <http://www.airccse.org/journal/ijdps/papers/0712ijdps19.pdf>.

[15] POLÁK, Ladislav and Tomas KRATOCHVIL. Simulation and Measurement of the Transmission Distortions of the Digital Television DVB-T/H Part 2: Hierarchical Modulation Performance. *Radioengineering* [online]. 2010, vol. 19, no. 4, pp. 703-711 [cit. 2019-05-01]. ISSN 1805-9600.

[16] Additive White Gaussian Noise (AWGN). *Wirelesspi.com* [online]. [cit. 2019-05-01]. Available at: <https://wirelesspi.com/additive-white-gaussian-noise-awgn/>.

[17] Rayleigh Fading. *Electronics-notes.com* [online]. [cit. 2019-05-01]. Available at: <https://www.electronics-notes.com/articles/antennas-propagation/propagation-overview/rayleigh-fading.php>.

[18] CIBULKA, Tomáš. *Simulation of the DVB-C and DVB-C2 transmission and their comparison.* Brno: Brno university of technology. Faculty of electrical engineering and communication. Department of radio electronics, 2013, 57 pages.

[19] JURÁK, Petr. *Model of physical layer of communication system IEEE 802.11ah.* Brno: Brno university of technology. Faculty of electrical engineering and communication. Department of radio electronics, 2018, 49 pages.

[20] Sure, Pallaviram and Chandra Mohan Bhuma. A survey on OFDM channel estimation techniques based on denoising strategies. *JESTECH* [online]. 2017, vol. 20, no. 2, pp. 629-636 [cit. 2019-05-01]. ISSN 2215-0986.

[21] MATLAB documentation. *MathWorks.com* [online]. [cit. 2019-05-01]. Available at: <`http://www.mathworks.com/help/`>.

List of symbols, physical constants and abbreviations

AP	Access Point
AWGN	Additive White Gaussian Noise
BSS	Basic Service Set
CAQ	Channel Availability Query
CSD	Cyclic Shift Diversity
CSM	Channel Schedule Management
CVS	Contact Verification Signal
DC	Direct Current
DFT	Discrete Fourier Transform
ETSI	European Telecommunications Standards Institute
FEC	Forward Error Correction
FCC	Federal Communications Commission
FFT	Fast Fourier Transform
GDB	Geolocation Database
GDD	Geolocation-Database-Dependent
IEEE	Institute of Electrical and Electronics Engineers
IDFT	Inverse Discrete Fourier Transform
IFFT	Inverse Fast Fourier Transform
IoT	Internet of Things
ISI	Inter-Symbol Interference
ISM	Industrial, Scientific and Medical
LDPC	Low-Density Parity-Check
LSB	Least Significant Bit
MAC	Medium Access Control Sublayer
MCS	Modulation and Coding Scheme
MIMO	Multiple-Input-Multiple-Output
MISO	Multiple-Input-Single-Output
MU	Multi-User
MU-MIMO	Multi-User Multiple-Input-Multiple-Output
non-HT	Non High Throughput
NCC	Network Channel Control
NDP	Null Data Packet
OFDM	Orthogonal Frequency Division Multiplexing
PHY	Physical Layer
PI	Pedestrian Indoor

PPDU	Physical Layer Protocol Data Unit
P/S	Parallel to Serial Converter
PSDU	Physical Layer Service Data Unit
PSK	Phase Key Shifting
QAM	Quadrature Amplitude Modulation
RF	Radio Frequency
RLSS	Registered Location Secure Server
RLQP	Registered Location Query Protocol
RRC	Root Raised Cosine
SIMO	Single-Input-Multiple-Output
SISO	Single-Input Single-Output
S/P	Serial to Parallel Converter
STA	Station
STBC	Space-Time Block Coding
SU-MIMO	Single-User Multiple-Input-Multiple-Output
TV	Television
TVHT	Television Very High Throughput
TVWS	TV White Spaces
UHF	Ultra High Frequency
VHF	Very High Frequency
VHT	Very High Throughput
W	Width
Wi-Fi	Wireless-Fidelity
WLAN	Wireless Local Area Network
WSD	White Space Device
WSM	White Space Map
ZF	Zero Forcing

A, B	convolutional encoder output bits
$A_{\mathrm{i}}, B_{\mathrm{i}}$	convolutional encoder output bits
B	channel bandwidth
C	square matrix of the discrete channel response samples
c_{k}	channel response sample in equalization
d	output complex symbol
f_{c}	carrier frequency
f_{d}	maximum Doppler frequency shift
$f_{\mathrm{d_{ratio}}}$	Doppler frequency ratio
f_{s}	symbol frequency
F_{s}	sample frequency

$F(z)$	frequency response function
g_{k}	equalizer coefficient
G_0, G_1	generator polynomial's coefficients in convolutional encoder
$h_{\mathrm{n,m}}$	channel matrix coefficient
H	channel matrix
i	index for the first and second permutations
I	in-phase axis
j	index after second permutation
k	index before first permutation
K	Rician factor
K_{MOD}	normalization factor
M	number of data streams
n_{k}	noise sample in equalization
$n[k]$	AWGN channel noise sample
N_{BPSC}	number of coded bits per subcarrier
N_{CBPS}	number of coded bits per OFDM symbol
N_{COL}	number of columns in interleaver block
N_{DBPS}	number of data bits per OFDM symbol
N_{e}	number of the reflected signals
N_{GI}	number of GI samples per OFDM symbol
N_{OFDM}	number of subcarriers per OFDM symbol
N_{r}	number of receiving antennas
N_{ROW}	number of rows in interleaver block
N_{SD}	number of complex data numbers per BCU
N_{SP}	number of pilot values per BCU
N_{SR}	highest data subcarrier index per BCU
N_{ST}	total number of subcarriers per BCU
N_{T}	number of transmitting antennas
Q	quadrature axis
r_{k}	received sample by the equalizer
R	coding rate
s	number for calculations in interleaver
s_{i}	coefficient of the transmission matrix in STBC
s_{k}	transmitted sample in equalization
$S_{\mathrm{i,j}}$	transmission matrix in STBC
SN	signal to noise ratio
$S(x)$	generator polynomial in scrambler
t	time
T	time slot

T_{DFT}	IDFT/DFT period
T_{GI}	guard interval duration
T_{GIS}	short guard interval duration
v	receiver speed
x	variable of generator polynomial in scrambler
$x[k]$	AWGN channel input sample
X	constant defined by regulatory domain
X_{i}	source data bit in convolutional encoder
y_{i}	decoded data bit in convolutional encoder
$y[k]$	AWGN channel output sample
$y(t)$	output signal of channel model
ρ_0	attenuation in the line of sight
ρ_{i}	attenuation on the reflection path
τ_{i}	relative delay on the reflection path
θ_{i}	phase rotation on the reflection path
Δf	subcarrier frequency spacing
$\otimes$	convolution operation

B	bytes
dB	decibel
GHz	gigahertz
kHz	kilohertz
km/h	kilometers per hour
$Mbit/s$	megabits per second
$Mbps$	megabits per second
MHz	megahertz
rad	radian
μs	microseconds

List of appendices

A Parameters for VHT mode **85**

A.1 Timing-related constants 85
A.2 Modulation-dependent parameters 85
A.3 Number of rows and columns in the interleaver 85
A.4 First permutation rule 85
A.5 Second permutation rule 86
A.6 Pilots mapping for BCU 6 and 8 MHz 86
A.7 Pilots mapping for BCU 7 MHz 86
A.8 Data subcarriers mapping for BCU 6 and 8 MHz 86
A.9 Data subcarriers mapping for BCU 7 MHz 87

A Parameters for VHT mode

A.1 Timing-related constants

Parameter	6 MHz	7 MHz	8 MHz	Description
N_{SD}	108	108	108	Number of complex data numbers per BCU
N_{SP}	6	6	6	Number of pilot values per BCU
N_{ST}	114	114	114	Total number of subcarriers per BCU

A.2 Modulation-dependent parameters

MCS Index	Modulation	R	N_{BPSC}	N_{CBPS}	N_{DBPS}	Data rate (Mbps) for 6 or 7 MHz	Data rate (Mbps) for 8 MHz
0	BPSK	1/2	1	108	54	1.8	2.4
1	QPSK	1/2	2	216	108	3.6	4.8
2	QPSK	3/4	2	216	162	5.4	7.2
3	16-QAM	1/2	4	432	216	7.2	9.6
4	16-QAM	3/4	4	432	324	10.8	14.4
5	64-QAM	2/3	6	648	432	14.4	19.2
6	64-QAM	3/4	6	648	486	16.2	21.6
7	64-QAM	5/6	6	648	540	18.0	24.0
8	256-QAM	3/4	8	864	648	21.6	28.8
9	256-QAM	5/6	8	864	720	24.0	32.0

A.3 Number of rows and columns in the interleaver

Parameter	TVHT_MODE_1	TVHT_MODE_2C, TVHT_MODE_2N	TVHT_MODE_4C, TVHT_MODE_4N
N_{COL}	18	27	48
N_{ROW}	$6 \times N_{BPSC}$	$8 \times N_{BPSC}$	$9 \times N_{BPSC}$

A.4 First permutation rule

$$i = N_{ROW} \times (k \bmod N_{COL}) + \lfloor k/N_{COL} \rfloor, k = 0, 1, ..., N_{CBPS} - 1 \qquad \text{(A.1)}$$

A.5 Second permutation rule

$$i = s \times \left\lfloor \frac{i}{s} \right\rfloor + \left(i + N_{CBPS} - \left\lfloor \frac{N_{COL} \times i}{N_{CBPS}} \right\rfloor \right) \bmod s, i = 0, 1, ..., N_{CBPS} - 1 \quad \text{(A.2)}$$

A.6 Pilots mapping for BCU 6 and 8 MHz

Channel configuration	Pilot indexes
TVHT_MODE_1	{-53,-25,-11,11,25,53}
TVHT_MODE_2C	{-125,-102,-83,-61,-42,-19,19,42,61,83,102,125}
TVHT_MODE_2N	{-53,-25,-11,11,25,53} for each BCU
TVHT_MODE_4C	{-269,-246,-227,-205,-186,-163,-125,-102,-83,-61,-42,-19, 19,42,61,83,102,125,163,186,205,227,246,269}
TVHT_MODE_4N	{-125,-102,-83,-61,-42,-19,19,42,61,83,102,125} for each BCU

A.7 Pilots mapping for BCU 7 MHz

Channel configuration	Pilot indexes
TVHT_MODE_1	{-53,-25,-11,11,25,53}
TVHT_MODE_2C	{-137,-114,-95,-73,-54,-31,31,54,73,95,114,137}
TVHT_MODE_2N	{-53,-25,-11,11,25,53} for each BCU
TVHT_MODE_4C	{-305,-282,-263,-241,-222,-199,-137,-114,-95,-73,-54,-31, 31,54,73,95,114,137,199,222,241,263,282,305}
TVHT_MODE_4N	{-137,-114,-95,-73,-54,-31,31,54,73,95,114,137} for each BCU

A.8 Data subcarriers mapping for BCU 6 and 8 MHz

Mode	Data indexes
TVHT_MODE_1	-58 : -2, 2 : 58
TVHT_MODE_2C	-130: -74, -70: -14, 14 : 70, 74 : 130
TVHT_MODE_2N	-58 : -2, 2 : 58 for each BCU
TVHT_MODE_4C	-274 : -218, -214 : -158, -130: -74, -70: -14, 14 : 70, 74 : 130, 158 : 214, 218 : 274
TVHT_MODE_4N	-130: -74, -70: -14, 14 : 70, 74 : 130 for each BCU

A.9 Data subcarriers mapping for BCU 7 MHz

Mode	Data indexes
TVHT_MODE_1	-58 : -2, 2 : 58
TVHT_MODE_2C	-142: -86, -82: -26, 26 : 82, 86 : 142
TVHT_MODE_2N	-58 : -2, 2 : 58 for each BCU
TVHT_MODE_4C	-310 : -254, -250 : -194, -142: -86, -82: -26, 26 : 82, 86 : 142, 194 : 250, 254 : 310
TVHT_MODE_4N	-142: -86, -82: -26, 26 : 82, 86 : 142 for each BCU